Quantum Well Intermixing by Ion Implantation

Anne Barnett

A thesis submitted in part fulfilment of the requirements for the degree of
Bachelor of Science (Honours)
The Australian National University

November, 2002

Declaration

This thesis is an account of research undertaken between July 2002 and November 2002 at The Department of Electronic Materials Engineering, Research School of Physical Sciences and Engineering, The Australian National University, Canberra, Australia. Except where acknowledged in the customary manner, the material presented in this thesis is, to the best of my knowledge, original and has not been submitted in whole or part for a degree in any university.

Anne Barnett
November 2002

Acknowledgements

A project of this magnitude would not have been possible without help and guidance from many people.

To my two supervisors, Prof. Jagadish and Dr Hoe Tan, thank you so much for all your ideas, words of wisdom and patience. Thank you Hoe for running up and down four flights of stairs every time I had a problem in the lab!

The large amount of experimental work carried out in this project using no less than five experimental set-ups has only been possible due to the on going technical support from Mr Michael Aggett, Mr Tony Watt, Mr Alan Hayes and Mr Tom Halstead, thank you.

Thanks is also extended to Prof. Mike Gal, from the University of New South Wales' Department of Condensed Matter Physics for allowing me access to their PL lab, and to Peter Reece for all his hands-on help and advice.

To all the staff and students in EME, thank you for being so friendly and helpful and for making my time here so enjoyable. Thanks especially to Dr Fu Lan for taking me under your wing last summer and showing me the workings of EME and also to Penny Lever for helping me with PL work in Sydney.

Thanks to Dr. Craig Savage for your excellent co-ordination of the honours program, and to my lecturers for your time, inspiration and assignment help!

To the honours students and various PhDer's in both RSPhysSE and the faculties, thanks for ensuring my year was a good balance of work and play and for introducing me to that fantastic stress reliever, mountain biking.

And lastly but by no means least, thank you to my parents for their unwavering support from abroad, and to Matt for putting up with all my stress.

I have had a fantastic year, and have no regrets about changing country or university despite negative forewarning's.

Thank you everyone.

Abstract

The development of semiconductor epitaxial growth techniques in the 1980's allowed the realisation of reproducible fabrication of semiconductor Quantum Wells (QWs) as first envisaged by Esaki and Tsu in 1970 [1]. Since then, QW heterostructures were found to have many interesting and varied properties of use in many industrial applications especially in the field of optoelectronics.

The work carried out in this study explored the phenomenon of ion implantation induced intermixing in QW structures. Two QW systems were investigated, the unstrained GaAs/$Al_xGa_{(1-x)}$As system and the strained $In_xGa_{(1-x)}$As/GaAs system. Previous results from proton (H) and Arsenic (As) implantation into these systems were verified, and new work on Boron (B) implantation was conducted to test the medium mass ion regime.

The fundamentally different nature of low and high mass ion implantation was confirmed in the studies of H and As implanted GaAs/$Al_xGa_{(1-x)}$As. A saturation effect in the high mass ion implantation was observed with increasing dose. The low mass ions did not show any energy shift saturation as dose was increased, for the range of implantation doses studied. B implantation produced a surprisingly small energy shift for all implant doses. It is proposed that either strain effects caused by the incorporation of B into the lattice, or the binding of B to point defects is responsible for the lower than expected shifts. Further investigations on the shifts exhibited by other medium mass ion species, (C and Al for example) are required. Temperature dependent implantation into the GaAs/$Al_xGa_{(1-x)}$As system was performed for the three ion species. The results for H showed a decrease in energy shift with temperature increase due to dynamic annealing taking place during the implantation process. The As results showed only a slight increase in shift with temperature due to the higher thermal stability of the implantation defects in the form of clusters. Boron showed no dependence on shift with temperature, indicating a competing effect between release of point defects from clusters, and annihilation of point defects due to dynamic annealing.

Preliminary investigations into the strained $In_xGa_{(1-x)}$As/GaAs QW system were carried out. Two QW systems were grown, one containing 30% In and one 50% in the barrier layers. The importance of strain in intermixing was exemplified in the results, with the dose dependent shifts for all three ion species being shown to be much reduced compared with the shifts gained from the unstrained GaAs/$Al_xGa_{(1-x)}$As system. The results for Boron showed this especially, with both blue and red shifts being observed. This was explained by competing mechanisms where a red shift from compressive strain relaxation during annealing counteracted the blue shift from the atomic interdiffusion, resulting in low overall energy shifts.

Further work is required to fully investigate the mechanisms involved in Boron implantation into the GaAs/$Al_xGa_{(1-x)}$As system, including comparison with other medium mass ion species. The effect of large strain in the $In_xGa_{(1-x)}$As/GaAs QW system due to high In content in the barriers was only briefly investigated, and further work is warranted.

Contents

Declaration iii

Acknowledgements v

Abstract vii

1 Introduction 1

2 Introductory Physical Concepts 3
2.1 Quantum Wells 3
2.2 Energy Band Structure 5
2.3 Semiconductor properties 6
2.4 Defects and Quantum Well Intermixing 7
2.5 Predictive Process Simulation 8

3 Experimental Techniques 11
3.1 Metalorganic Chemical Vapour Deposition 11
3.2 Ion Implantation 13
3.3 Rapid Thermal Annealing 15
3.4 Photoluminescence Spectroscopy 15

4 The GaAs/AlGaAs QW System
Results and Discussion 19
4.1 Experimental 19
4.2 Results 20
4.2.1 *Experimental* 20
4.3 Discussion 23
4.3.1 *Dose dependence* 23
4.3.2 *Temperature Dependence* 29

5 The InGaAs/GaAs QW System
Results and Discussion 35
5.1 Experimental 35
5.2 Results 35
5.2.1 *Experimental* 35
5.3 Discussion 37
5.3.1 *Dose dependence* 37

6 Conclusion 39

List of Figures

2.1 The ground state energy (dashed) resulting from the fabrication of a QW heterostructure, showing the quantised ground state energy bandgap E_g . . 4
2.2 The quantised energy level of a GaAs/AlGaAs QW heterostructure, showing the conduction band levels at the top and the valence band levels at the bottom. L is the width of the QW layer (Adapted from reference [17]) . . . 4
2.3 Energy band structure of the three material classes, showing energy bandgap E_g in semiconductors and insulators. (Adapted from reference [18]). 5
2.4 The Zinc-blende lattice structure of III-V semiconductors, (Adapted from reference [18] 7
2.5 Well changes induced by QW Intermixing, (a) represents an "as-grown" square well, and (b) shows the rounded intermixed well shape. Note the increase in energy gap of the energy level E_0 in the intermixed case. 7

3.1 Schematic of the EME MOCVD machine used to grow the QW's 12
3.2 Diagram of the EME High Energy Ion Implanter 14
3.3 The emission of a photon (energy $E = hv$) from recombination of a conduction electron (a) and a valence hole (b) (Adapted from reference [21] 15
3.4 A typical PL experimental setup (Adapted from reference [22] 16
3.5 A typical PL experimental result spectra showing energy peaks corresponding to the ground state energy of as-grown QW's in the sample. 17

4.1 TRIM damage profile simulation with the position of the three QWs studied shown. 20
4.2 12K PL spectra for H implanted GaAs/AlGaAs 21
4.3 12K PL spectra for B implanted GaAs/AlGaAs 22
4.4 12K PL spectra for As implanted GaAs/AlGaAs 22
4.5 Implantation energy shift as a function of dose for H 23
4.6 Implantation energy shift as a function of dose for B 24
4.7 Implantation energy shift as a function of dose for As 24
4.8 Schematic showing the effects of well width on shifting levels. 26
4.9 Repeated results for implantation energy shift as a function of dose for B - High Energy implanter 27
4.10 B implanted GaAs/AlGaAs dose dependent shift results; reannealed (ra) at 950^{0}C for 60s 28
4.11 77K PL spectra for H temperature dependent GaAs/AlGaAs 29
4.12 77K PL spectra for As temperature dependent GaAs/AlGaAs 30
4.13 Implantation energy shift as a function of temperature for H 31
4.14 Implantation energy shift as a function of temperature for As 32
4.15 77K PL spectra for B temperature dependent GaAs/AlGaAs 32
4.16 Implantation energy shift as a function of temperature for B 33

5.1 Annealing temperature study results for the $In_xGa_{1-x}As/GaAs$ QW system 36
5.2 Dose dependent energy shift results for B implanted $In_xGa_{1-x}As/GaAs$ QW system . . . 37
5.3 Schematic showing the effect of strain on semiconductor energy bands . . . 38

Chapter 1

Introduction

In 1729, the English scientist Stephen Gray showed that different materials exhibit different electric flow properties, specifically some tended to easily transmit electric flow, while others resisted it [2]. The materials studied all seemed to fall into one of two categories; conductor or insulator.
It wasn't until nearly a century later in 1821 that Thomas Seebeck first discovered some properties of the compound PbS that did not fit entirely into either category. Further work on these remarkable materials was performed by the likes of Michael Faraday who in 1833 reported a conductivity temperature dependence for the class of new materials [3]. This was the first observation of the properties of a special class of materials known as *semiconductors*. The most well known semiconductor (Silicon) was isolated and identified by John Berzelius in 1924 and in the years that followed many complex devices were designed and fabricated out of semiconductors. The silicon p-n junction (1940), the bipolar junction transfer resistor or transistor (1947) for which Shockley, Bardeen and Brattain received the 1956 Nobel prize in physics, the integrated circuit (1958), the MOSFET (1960), CMOS technology (1963) and the subsequent miniaturisation and integration of these and many other semicondutor devices have resulted in the complete and unimpeeded adoption of semiconductors into almost every facet of modern electronic technologies [4].

An important step in the understanding of the physical properties of semiconductors came with the bandgap model of material energy levels, when a young Swiss physicist Felix Bloch first created a theory of electronic band-gap structures in solids in 1928 [5]. This was done by solving the Schrödinger equation for the infinite number of interacting electrons moving in the static field of an infinite number of ions in a material, by simplifying it to a one electron approximation.

Since then there have been many developments in both the theory of semicondutor materials and in the subsequent application of semiconductors to modern electronic devices. The development of novel techniques for material manipulation has been an important part of this rapid application.

Ion implantation first appeared in the late 1940's when R.S. Ohl and W. Shockley, two research scientists working at Bell Telephone Laboratories in the United States, found that optical patterning methods used in microelectronics were becoming unreliable and the resolution of patterns under two microns was impossible. In 1954 Shockley patented ion beam production of buried base layers in bipolar transistors as an alternative method to diffusion in forming transistor junctions. The early applications of ion beams to the microelectronics industry were for etching and deposition, and more recently ion beams have been used for reactive processes, doping and material property modification for op-

toelectronic applications.

The first attempts at QW heterostucture fabrication were made by Arthur and Cho at the Bell Laboratories in the United States at the end of the 1960's using the method of Molecular Beam Epitaxy (MBE), however the first reproducible growths were achieved with the advent of commercial growth machines in the 1980's [6]. The manipulation of these heterostuctures by inducing the barrier and well atoms to interdiffuse was found to be a very powerful mechanism whereby the energy bandgaps of the active well layers could be controlled.

A number of techniques have been developed to induce quantum well intermixing. As well as ion implantation, impurity induced layer disordering, impurity free vacancy diffusion (dielectric capping techniques) and laser induced intermixing have been reported [7] - [13]. Ion implantation is particularly suited over other techniques in the manipulation of quantum wells for optoelectronics applications due to its high reproducibility and controlability, and its ability to easily induce intermixing at deeper regions of a heterostructure.

The study of the relationship between intermixing mechanisms and implantation parameters formed a major part of the work carried out by Dr Fu Lan and Dr Hark Hoe Tan in their PhD studies in the Electronic Materials Engineering Department of the Research School of Physical Sciences and Engineering at the Australian National University[14],[15]. The implantation of low mass ions (Protons) and high mass ions (Arsenic) into unstrained ($GaAs/Al_xGa_{(1-x)}As$), and strained ($In_xGa_{(1-x)}As/GaAs$ and $In_xGa_{(1-x)}As/AlGaAs$) quantum well (QW) systems was carried out and extensive study was undertaken into understanding the nature and evolution of the material defects involved in the intermixing results obtained.

The work presented in this thesis has been specifically designed to follow on and extend their work. An investigation of the effects of medium mass ion implantation was carried out by implanting Boron ions into the $GaAs/Al_xGa_{(1-x)}As$ and $In_xGa_{(1-x)}As/GaAs$ QW systems, using a variety of implantation conditions. The extent of the intermixing in each case was investigated using optical excitation methods. The investigation of a medium mass ion was specifically chosen to connect the findings of Proton and Arsenic implantation which showed that fundamentally different intermixing mechanisms exist for low and high mass ions.

This thesis firstly presents an outline of physical concepts relevant to semiconductors and QW intermixing, followed by an outline of the experimental techniques employed in this study. Theoretical and experimental results are presented followed by an in depth discussion.

Chapter 2

Introductory Physical Concepts

The full understanding and subsequent physical development of new semiconductor devices is only achieved by careful consideration of the physical principles that govern semiconductor material's properties and how these can be manipulated. This chapter is devoted to the introduction of relevant terms and concepts that pertain to this purpose.

2.1 Quantum Wells

The theoretical idea of a Quantum Well (QW) is first presented to most undergraduate physics students as a rectangular well stucture with a finite energy barrier sandwiching a zero energy well region. The energy levels within the well are quantised with a lowest eigen-energy value and may be gained by solving the Schrödinger Equation for a finite potential well.

In solid state studies, a QW is a tri-layered semiconductor device, the middle 'well' layer being made of a smaller energy band gap material than the two outside 'barrier' layers. The QW's studied in this work are all made with the well material having a lower energy bandgap than the barrier layers, and the bands are aligned in such a way that the conduction band of the barrier layers is of higher energy relative to the well layer, and the barrier valence band energy is also relatively lower than that of the well layer.
As the active layers of a heterostucture (in this case the well layers) become sufficiently close to the De-Broglie wavelength of the carriers in the well (about 1 -10nm), quantum effects in the motion of the electrons within the heterostucture are observed and the well must be described with quantum mechanical concepts, where the energy levels within the well have discrete (quantised) values. This is known as the quantum size effect. The carriers in the well layer now respond in the same way as a carrier in a finite barrier potential well. The lowest energy eigenvalue (ground state energy) of the carriers in the conduction band is raised above the bottom of the well, (the highest energy level for holes in the valence band also drops), resulting in an increase in energy bandgap between the conduction and valence bands of the material (figure 2.1). One may control this energy bandgap widening by varying well thickness (see equation 2.1) and/or barrier constituents.

For a semiconductor the Schrödinger equation for a particle in a one-dimensional box with finite barriers can be numerically solved. However for simplicity the application of the Schrodinger equation and its solutions for an infinitely deep potential results in the expression for the eigen-energies as in Devices"[16]. The resulting expression for the eigen-energies is:

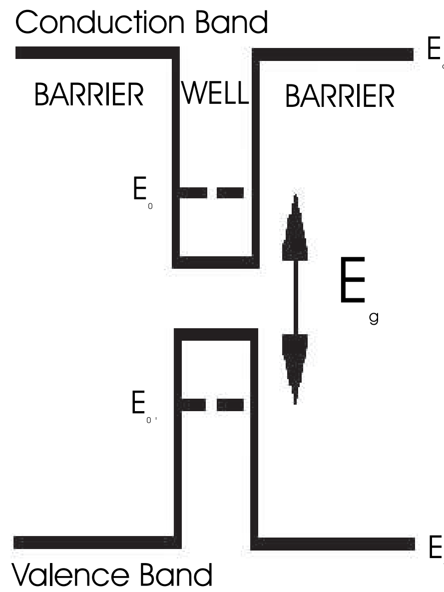

Figure 2.1: The ground state energy (dashed) resulting from the fabrication of a QW heterostructure, showing the quantised ground state energy bandgap E_g

$$E_n = \frac{E_g}{2}[(1 + \frac{4E_0 n^2}{E_g})^{\frac{1}{2}} - 1] \tag{2.1}$$

with n=1,2,3,... and E_0 being the ground state energy, given by $E_0 = \frac{\pi^2\hbar^2}{2mL^2}$, where L is the QW thickness.
A diagram showing the evergy levels formed in a GaAs/AlGaAs QW heterostructure is shown in figure 2.2.

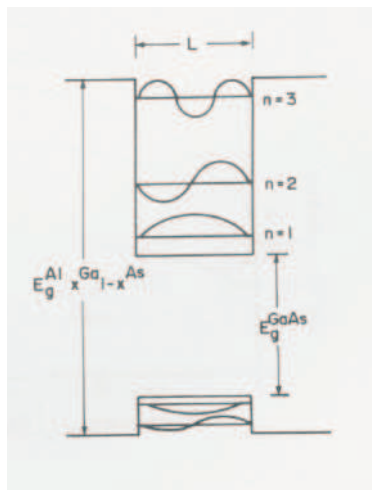

Figure 2.2: The quantised energy level of a GaAs/AlGaAs QW heterostructure, showing the conduction band levels at the top and the valence band levels at the bottom. L is the width of the QW layer (Adapted from reference [17])

2.2 Energy Band Structure

One of the fundamental properties of a semiconducting material is its energy band structure, that in a semiconductor describes the variation of energy, E, in the material with wavevector $\vec{k}$. The energy bands of the periodic lattice structure of the material result from the overlapping of the four valence electron orbitals, one s-type and three p-type, between nearest neighbour atoms. Due to the periodicity of the lattice structure, this results in a number of allowed energy bands for the valence electrons and there is a region of disallowed energies between the valence energy level (highest filled energy level at zero temperature) and conduction energy level (lowest unfilled energy level at zero temperature). In order for a material to conduct electricity, electrons must be excited over this energy gap between valence and conduction bands and it is the height of this gap that determines whether the material will be a conductor, an insulator or somewhere in between. These properties are illustrated in the diagram showing schematics of the three material classes (Figure 2.3). Metals have an overlap between their conduction and valence bands allowing easy flow of electricity. In a insulator, the valence-conduction gap is so large that essentially no electrons are present in the conduction band. Semiconductors however have an electronic excitation band gap of between 0 and 4 eV, which is small enough to allow some electrons to be thermally excited into the conduction band when they gain thermal energy of $E = kT$ greater than or equal to E_g.

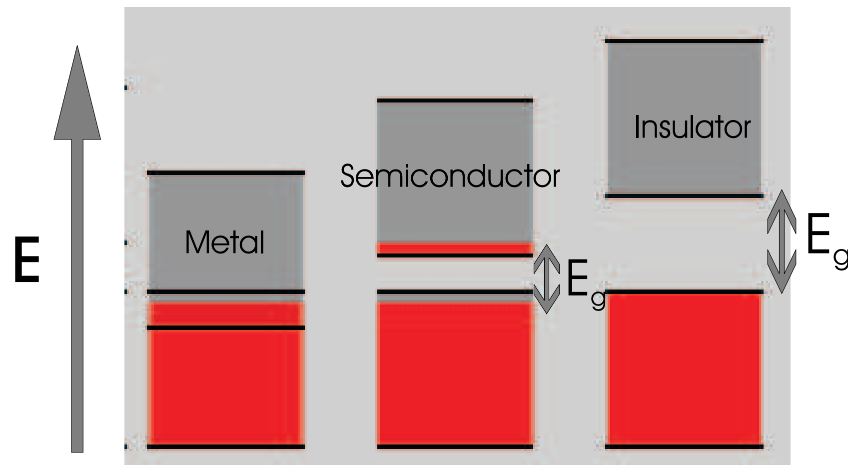

Figure 2.3: Energy band structure of the three material classes, showing energy bandgap E_g in semiconductors and insulators. (Adapted from reference [18]).

As mentioned in the introduction, the development of electronic bandgap theory began in 1928 when Felix Bloch solved the one electron Schrödinger equation:

$$[\frac{\mathbf{p}^2}{2m} + V(\mathbf{r})\psi(\mathbf{r})] = E\psi(\mathbf{r}) \tag{2.2}$$

The solutions for the electronic band energies, E, incorporate the interaction of a single electron with all the other electrons in the lattice, through the periodic crystal potential V($\mathbf{r}$). Although at first sight the approximation based on a single electron in what is obviously a many particle system may seem very simple, it was employed sucessfully to explain many important results such as that obtained by A.H. Wilson, published in 1954, where he explains the distinction between a conductor, a semiconductor and an insulator in the solid state, based on the one electron approximation above [19].

The three main methods developed since 1928 of calculating semiconductor energy bands are the pseudopotential method, the linear combination of atomic orbitals or tight binding method, and the $\vec{k}.\vec{p}$ method. The reader is refered to "Modern Semiconductor Quantum Physics" for full energy bandgap structure derivations by each of these methods[20].

2.3 Semiconductor properties

The first references to bandgap engineering by alloying of materials was made in 1970 by L. Esaki and R.Tsu where they proposed not only the possibility of mixing together semiconductors from groups III and V or groups II and IV to make alloy materials with specific energy bandgaps, but also introduced the idea of growing planar layered semiconductor structures for optoelectronic applications[1]. Alloy materials of group III and group V semiconductors were used as the barrier and well layers of the QW's grown in this study.

Semiconductors come in a variety of types, elemental, binary, ternary, quaternary, layered and organic to name just a few.

Elemental semiconductors are semiconductors where each atom is of the same type such as group IV elements Ge or Si. These atoms are bound together by covalent bonds, so that each atom shares an electron with its nearest neighbour, forming strong bonds. These materials all have the disadvantage that they are indirect bandgap materials, where the top of the valence band does not line up with the bottom of the conduction band in an energy vs. wave number (E vs. **k**) diagram. This results in a loss in quantum efficiency as the electron must either have energy greater than that of the minimum bandgap or must gain (or lose) momentum through a three body process in order to move into the minimum energy level in the conduction band. As such, elemental semiconductors are not the best choice for optical applications.

Binary semiconductors are made of combinations of two elements. Common examples are GaAs or InP. These compound semiconductors belong to the III-V semiconductor group, so called because the two elements can be found in group III and group V of the periodic table respectively. These binary semiconductors have a difference in electro-negativity which leads to a combination of covalent and ionic bonding, and as a result have a direct bandgap structure, vertical transitions can take place from the top of the valence band into the minimum energy level in the conduction band without any change in the electron's momentum i.e. occur at $\mathbf{k} = 0$ or the Γ point. Hence III-V semiconductors have a much higher quantum efficiency than group IV semiconductors, leading to their frequent use in optical semiconductor devices.

Ternary semiconductors are formed by the addition of a third element to the mixture, for example $Al_xGa_{1-x}As$. The subscript x refers to the alloy content of the material, and indicates the proportion of each group III element.

The materials used in this study, (Binary and Ternary III-V compound semiconductors) have a zinc-blende lattice structure which consists of two interlocking face-centered cubic lattices (figure 2.4)

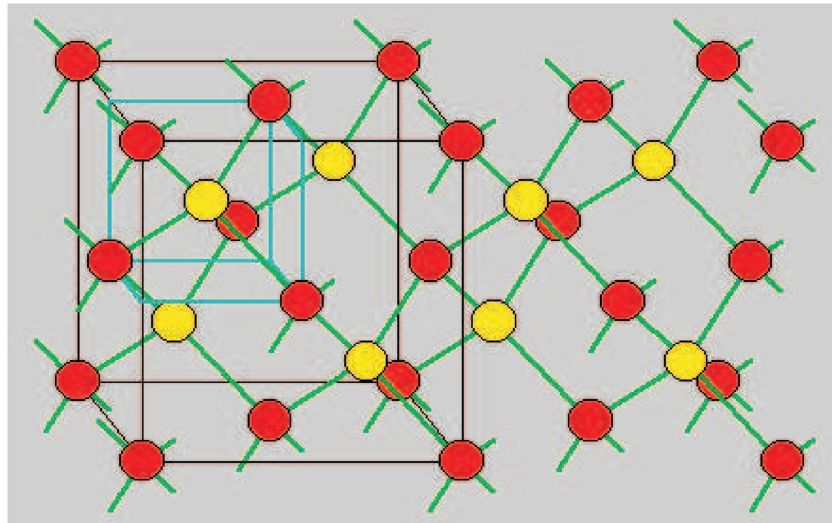

Figure 2.4: The Zinc-blende lattice structure of III-V semiconductors, (Adapted from reference [18]

2.4 Defects and Quantum Well Intermixing

The presence of grown-in and implantation induced defects in a material have important consequences for its physical and optical properties. The importance of understanding and manipulation of defects to the optoelectronics industry is reflected in the significant amount of research carried out over the last twenty years in defect and QW intermixing studies.

Ion implantation into a semiconductor imparts energy to the system, forming point defects (vacancies and interstitials) as well as extended and complex defects. These accumulate, resulting in an increase in the free energy of the system. During post-irradiation annealing, interdiffustion between vacancies and interstitials results in the annihilation of the extra point defects in the system and a reduction in its free energy. The result for a QW heterostucture is the migration of defects across the barrier-well interface as atoms migrate, swapping places with the point defects, resulting in interdiffusion of (in this study's case), the group III species, effectively intermixing the layers. This is the process of Quantum Well Intermixing (QWI) (figure 2.5).

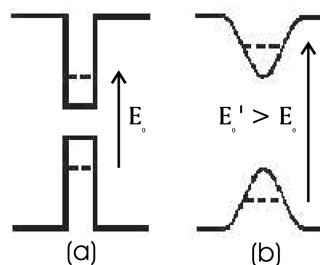

Figure 2.5: Well changes induced by QW Intermixing, (a) represents an "as-grown" square well, and (b) shows the rounded intermixed well shape. Note the increase in energy gap of the energy level E_0 in the intermixed case.

The extent to which QWI occurs depends upon the diffustion rates of the point defects.

The final well profile is normally assumed to follow a double error function profile given by

$$x(z) = x_0 \left\{ 1 + \frac{1}{2} erf(\frac{z - \frac{L_z}{2}}{2\sqrt{Dt}}) - \frac{1}{2} erf(\frac{z + \frac{L_z}{2}}{2\sqrt{Dt}}) \right\} \tag{2.3}$$

Where t is the annealing time, L_z the width of the QW, D is the interdiffusion coefficient, and x_0 is the initial concentration of one of the interdiffusing species.

In this study the extent of intermixing is determined in terms of the observed shifts in the photoluminescence spectrum relative to reference samples, which is the important factor when optoelectronics applications are considered.

2.5 Predictive Process Simulation

Before any ion implantation can take place, predictive process simulation must be carried out in order to determine the damage profiles for each ion species.

In order for reasonable comparisons to be made between different implantations, one must implant the ions with the correct energy and dose to produce similar damage (defect) profiles. The aim is to implant in such a way that the variation between defect density generated between the QWs is as small as possible. The doses must also be scaled so that the collisional displacement density generated by each ion species is the same.

The first attempt at predictive process simulation used simplified analytical models, however it was found that the use of atomic scale calculations connecting experimental data, first-principle calculations and kinetic models of material evolution at the atomic scale, produced a more accurate insight into the physical processes involved and allowed for a wider range of implantation variables. The most popular simulation technique used is the Monte Carlo technique.

The Monte Carlo program used in this study was TRIM (TRansport of Ions in Matter) v. '95. The program takes as input parameters, implantation ion species, mass and energy, layer constituents and their proportion of the sample material, the density of the material, the displacement energy of the material atoms, the binding energy of the lattice, and the angle of the incident ion beam to the sample. The program then simulates the trajectory of each implanted ion seperately, taking into account a number of assumptions. The first of these is to assume that the thermal energy of the target atoms is negligible compared to that of the implanted ions, thus no energy is transfered from the target atoms to the incident ion during the course of the implant. These thermal vibrations are modelled as displacements from the regular lattice structure.

After a collision between an implanted ion and a target atom has occured, there are four different options as to the type of defect formed:

1. If both the incident and the target atom end up with energies greater than the energy required to displace an ion from the lattice (the displacement energy), a *vacancy* is formed where the target atom was and both the particles become moving members of the cascade.

2. If the incident ion ends up with energy greater than the displacement energy, but

the target atom does not, the implanted ion will continue in the cascade, and the target atom will vibrate back to its original state releasing the energy imparted to it from the implanted ion as phonons.

3. If the incident ion does not end up with energy greater than the displacement energy, but the target atom does a *replacement* collision occurs. The defect will be an *antisite* if the implanted ion is a different species to the target atom, and if they are of the same species, the incident ion simply replaces the target atom and releases its execess energy in the form of phonons.

4. If both the implanted ion and the target atom end up with energies less than the displacement energy, the implanted ion stops in between the lattice points, creating an *interstitial* defect. The excess energy from both the implanted ion and the target atom is released as phonons.

The program then simulates the damage formed from a sufficient number of incident ions to give a good statistic and outputs profiles of point defect damage created per ion per Åvs. depth. By performing a number of simulations for each implantation ion species, it is possible to find energies that result in damage profiles with similar shapes and peaks where a similar damage profile for each ion is obtained.

Chapter 3

Experimental Techniques

The growth and processing of high quality materials is of vital importance to the semiconductor industry. All processes must be accurately controlled at each step, be easy and cheap to reproduce and result in a high quality product.

There are a number of processing options avaliable at each stage of the QW fabrication and manipulation process. The QW's used in this study were grown by Metalorganic Chemical Vapour Deposition (MOCVD) and manipulated using high and low energy Ion Implantation (II), followed by Rapid Thermal Annealing (RTA). The resulting QW's were analysed using low temperature Photoluminescence Spectroscopy (PLS) and Rutherford Backscattering Spectroscopy (RBS). The description of these techniques forms the basis for this chapter.

3.1 Metalorganic Chemical Vapour Deposition

The adoption of semiconductors as the choice material for the electronics industry resulted in subsequent advances and refinements of material growth techniques. Growth of bulk single crystals is usually carried out by either the Czochralski Method or the Bridgman Method, however since the growth of a large bulk crystal is rather expensive, the usual option is to grow a thin high quality crystal layer on top of a bulk crystal. The deposition of a thin semiconductor film on a substrate is the process of *Epitaxial Growth*. It is important that the substrate used has very similar, if not identical, lattice parameters to the epitaxial film, since the substrate causes the lattice of the film to grow with the same crystallographic orientation. A mismatch of lattice parameters would result in a large strain between the substrate and the film, and hence a low quality film would be produced.

The QW's used in this study were all grown using the process of epitaxial film deposition in the gaseous phase. They were grown on semi-insulating (100) GaAs substrates using the method of Metalorganic Chemical Vapour Deposition (MOCVD).

The process of an MOCVD growth involves a number of carefully controlled steps in order to produce a high quality sample. Before the main structure layers are grown, the substrate is heated up to 750^0C to remove and native oxide from the surface. The growth temperature is set (750^0C for this study) and a GaAs buffer layer of between 0.2 - 0.5 μ m is grown to smooth the surface. This is followed by the layers of the main structure. The exact growth time for each layer is taken from previous growths of known thickness and time. The barrier layers do not need to have such an acurate thickness and a linear

growth rate is assumed. It is important however to carefully control the composition of the barrier layers and this is done using mass flow controllers to control the gas flow ratio between constituent atoms. The total gas flow through the system must be maintained at a constant value throughout the various layer growths and “dummy” flows of Hydrogen are introduced where needed to maintain the constant value of the flow. As well as the flows, the pressure difference between the reactor and the vent line must be kept as close to zero as possible. The final layer grown is a capping layer to prevent oxidation of the layers below. Waste gases are scrubbed before being released.

The chemical reactions employed to grow a III-V semiconductor layer use vapour phase reactions between metal alkyls and hydrides. The three types of III-V layers grown in this study were GaAs, $Al_xGa_{1-x}As$ (x=0.54) and $In_xGa_{1-x}As$ (x = 0.3 and x = 0.5).

The corresponding chemical reactions are given by:

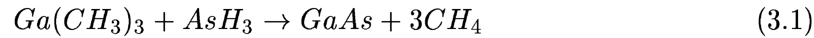

$$Ga(CH_3)_3 + AsH_3 \rightarrow GaAs + 3CH_4 \tag{3.1}$$

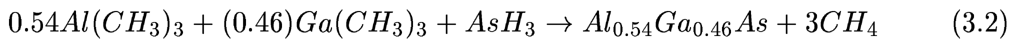

$$0.54Al(CH_3)_3 + (0.46)Ga(CH_3)_3 + AsH_3 \rightarrow Al_{0.54}Ga_{0.46}As + 3CH_4 \tag{3.2}$$

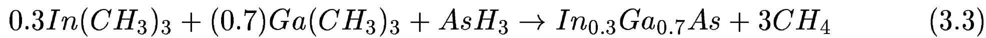

$$0.3In(CH_3)_3 + (0.7)Ga(CH_3)_3 + AsH_3 \rightarrow In_{0.3}Ga_{0.7}As + 3CH_4 \tag{3.3}$$

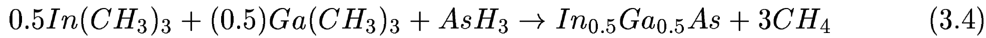

$$0.5In(CH_3)_3 + (0.5)Ga(CH_3)_3 + AsH_3 \rightarrow In_{0.5}Ga_{0.5}As + 3CH_4 \tag{3.4}$$

The unwanted methane is highly volatile, and is removed through the exhaust into the scrubber. A schematic of the MOCVD machine used in this study is shown in figure 3.1.

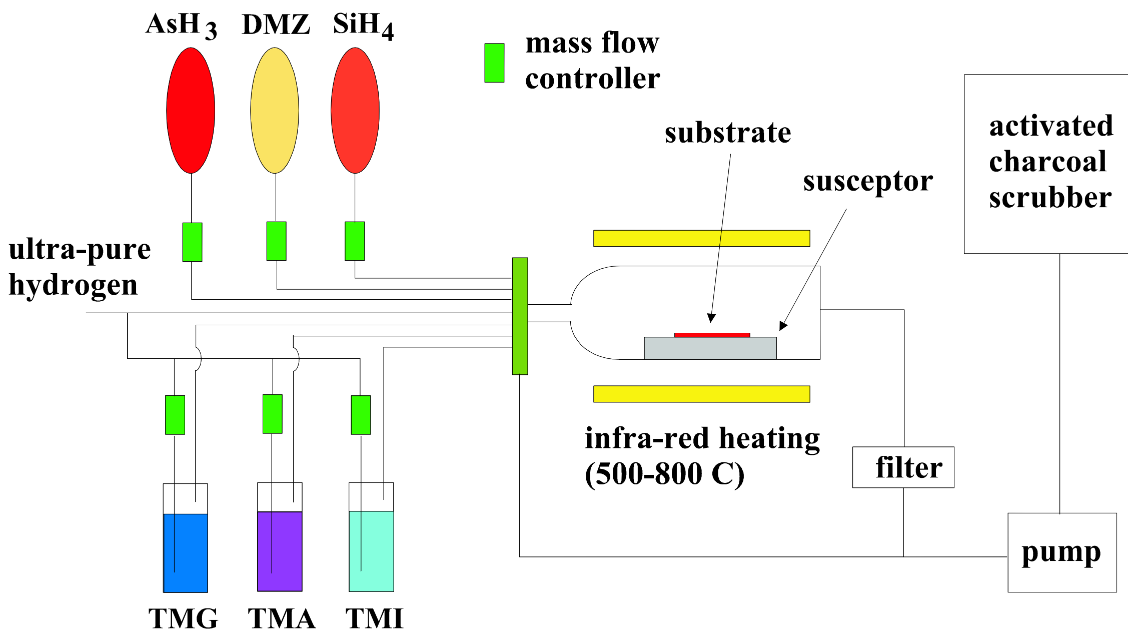

Figure 3.1: Schematic of the EME MOCVD machine used to grow the QW's

3.2 Ion Implantation

The process of ion implantation involves the ionisation of atoms or molecules which are then accelerated by an electric field and implanted into the target material.

A wide variety of combinations of target materials and implanted ions are possible. The dose of the implanted ions can be varied between 1×10^7 and 1×10^{17} cm^{-2}, and acceleration energies of between several keV and up to 10 MeV may be produced. The range of the implanted ions into the substrate depends on the mass of the implanted ions, their energy, the mass of the substrate atoms, the crystal structure and the angle of incidence of implantation beam to the target.

Within an ion implantation system, there are six main components, the ion source, the extractor, the ion analysing system, the accelerator, the scanner and the target chamber 3.2. Ions are produced from the source by applying a voltage between the source cathode and anode and inducing ions out of the source. The low energy implants carried out in this work use negative ions (H-, B-) from TiH and B sources and positive (As+) ions from a $GaAs$ source for the high energy implants. A Cesium oven is located at the source to introduce Cs ions into the beam to improve conductivity and help control sputtering. The resulting ions are accelerated away from the source area by extractor electrodes and bias coils. The potential across these may be varied to allow for different implantation energies.

The ion beam extracted from the source may contain many different ion species. An analysing magnet is thus employed to select the desired ion species.

The ions enter a homogeneous magnetic field directed normal to their path and the ions feel a force expressed by Faraday's law:

$$\vec{F} = q(\vec{v} \times \vec{B}) \tag{3.5}$$

Where $\vec{B}$ is the magnetic flux density, and $\vec{F}$, q and $\vec{v}$ are the force, charge and velocity of the ions respectively.

The ions follow a circular path with a centrifugal force $F = \frac{Mv^2}{r}$. Equating these two force expressions gives a radius of curvature for the ions of

$$r = \frac{Mv}{qB} \tag{3.6}$$

Since q and B are normal to each other, replacing $v = \frac{2E}{M}^{\frac{1}{2}}$ derived from the kinetic energy of the ions, and recall that the kinetic energy E of the ions is given by $E = qV$ for extraction voltage V:

$$r = \frac{2VM}{q}^{\frac{1}{2}}/B \tag{3.7}$$

Thus by varying the extraction voltage (V) and the magnetic field (B), any particular ion species may be selected by the magnet.

After the beam has been analysed, magnetic and electric fields are used to focus the naturally divergent ion beam. For high energy implantation, the ion beam is also passed

through an accelerator where the ions are further accelerated up to 10MeV. Nitrogen gas is injected into the accelerator, resulting in an exchange of charge for the ions in the beam from negative to positive, enhancing the acceleration. Since the ions now have new charge states, a switching magnet is employed after the acceleration phase to reselect the ion with the desired charge state.

The ion beam is then scanned in both x and y directions using electrostatic fields. A current integrator placed between the target and the ground outputs the total incident ion current, giving the total dose. From this a dose may be obtained.

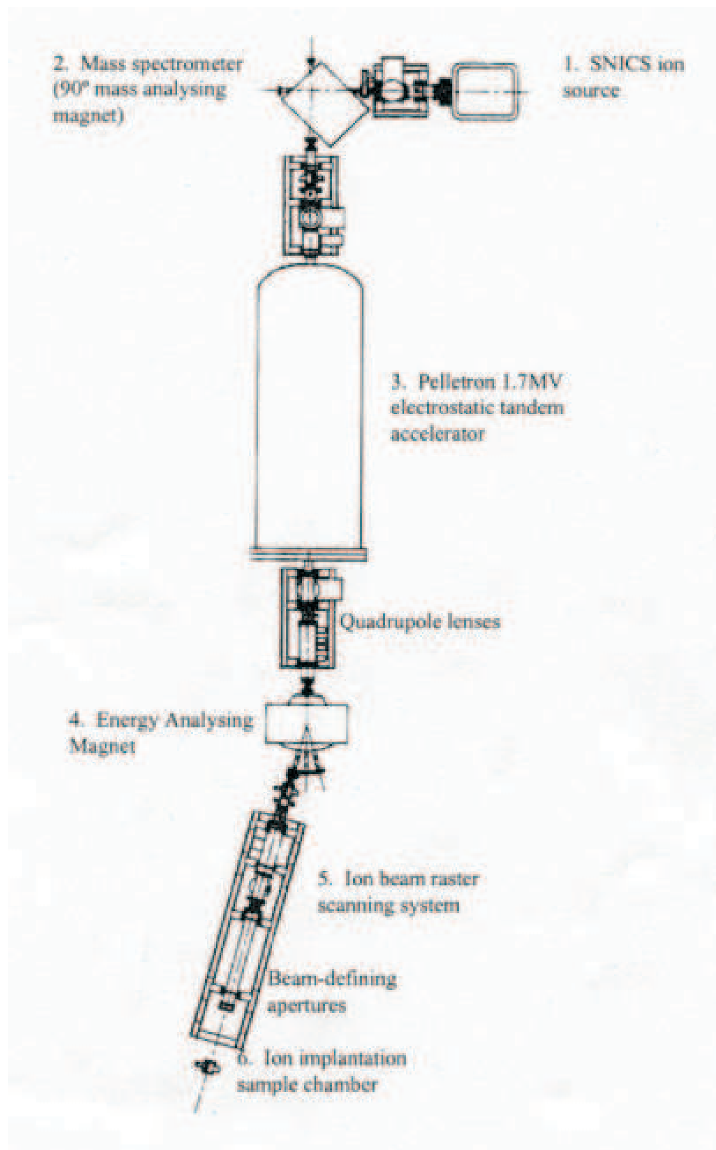

Figure 3.2: Diagram of the EME High Energy Ion Implanter

Ion implantation as a Quantum Well Intermixing (QWI) technique has a number of distinct advantages over other intermixing processes (for example dielectric capping). The most important of these are short processing times, good homogeneity and reproducibility of implantation profiles, exact control of the amount of implanted ions by electrically monitoring and then integrating the current, the ability to achieve large penetration depth

of the implanted ions (allowing for modification of areas far away from the surface of the target) and (by using sequences of implantation steps, with different energies and doses) the optimisation of dopant profiles.

3.3 Rapid Thermal Annealing

Ion implantation results in the creation of point defects, point defect clusters and extended defects. These defects are manipulated using post-irradiation Rapid thermal annealing (RTA). RTA promotes QWI in three distinct ways. Annealing a sample imparts thermal energy to the point defects within it, allowing them to migrate across the QW boundaries resulting in intermixing of the layers. Thermal energy also breaks up any point defect clusters, releasing many more point defects for intermixing. Annealing is also very important in the recovery of the material as it breaks up extended defects, removing non-radiative recombination centres and hence increasing the material quality.

The annealing carried out in this study was performed by an AET Rapid Thermal Processor using quartz lamps as the heating source. The samples were annealed under Ar flow for 30s, face down between two pieces of semi-insulating GaAs in order to prevent excess loss of As from the surface of the material (proximity method).

3.4 Photoluminescence Spectroscopy

The experimental steps described up to this point are all processing steps required to intermix the QW's. Characterisation techniques are now employed to determine the extent of the intermixing induced modification of the QW's and to measure the optical output quality of the material. The first technique employed is Photoluminescence Spectroscopy (PLS), which allows for non-destructive probing of the material's electronic structure. The term *luminescence* refers to light energy emitted by a body at a certain temperature, excluding thermal radiation. PLS uses a laser to excite valence electrons into the conduction band, resulting in a non-thermal equilibrium. Radiative recombination of the resulting electron-hole pairs to a thermal equilibrium state, results in the emission of a photon with energy (and wavelength) corresponding to the energy gap between the conduction electron and valence hole (see figure 3.3). Hence the luminescence from electron-hole recombination provides direct infomation on the bandgap stucture of the QW's.

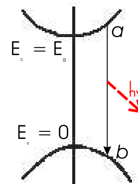

Figure 3.3: The emission of a photon (energy $E = hv$) from recombination of a conduction electron (a) and a valence hole (b) (Adapted from reference [21]

PLS is carried out under vacuum to avoid condensation and at low temperature to reduce evergy level broadening due to phonon interation. The excitation sources used were an Ar ion laser (514.5nm) for 12K and a solid state diode laser (532nm) for 77K. The luminescence was detected through a monochromator using either a Si or InGaAs photodetector.

An example of at typical PL experimental setup is shown in figure 3.4. The resulting luminescence plots shown energy peaks corresponding to QW's such as those in figure 3.5.

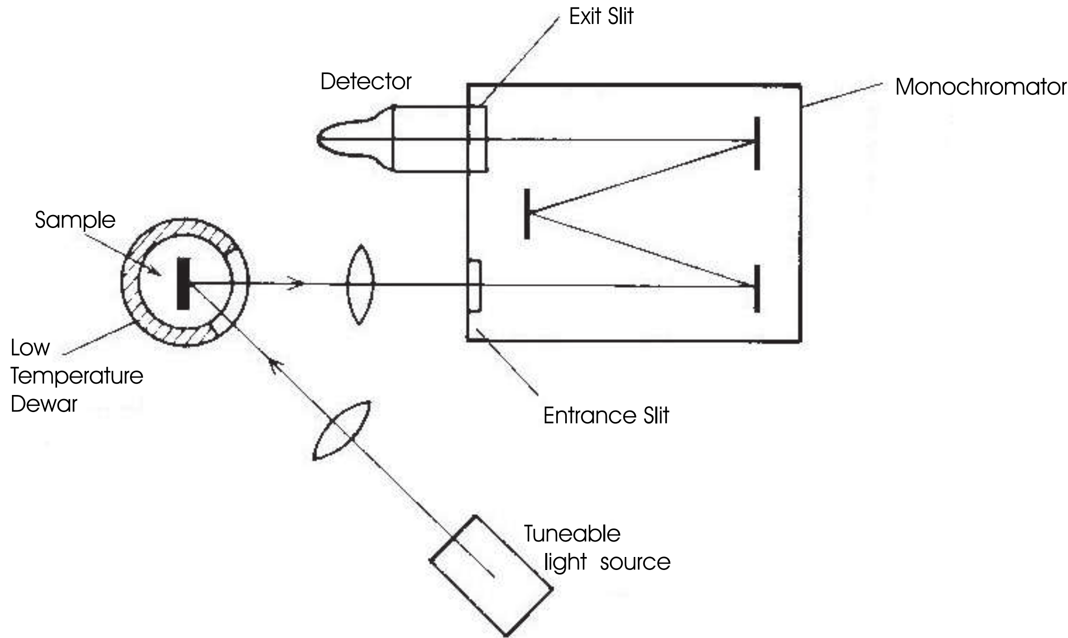

Figure 3.4: A typical PL experimental setup (Adapted from reference [22]

PLS has four main applications within the study of materials.

As described above, PLS is employed to determine bandgap energies by initiating excitations of electrons between the valence and conduction bands of a semiconductor, however PLS is also a powerful technique in the determination of material quality and in defect studies.

Defect studies utilising PLS involve the indentification of specific defects and determination of their concentration. This is done by identifying localised defect energy levels and observing the intensity of the corresponding PL output.

PLS is also used to identify electron-hole recombination mechanisms. The recombination process of conduction electrons with valence holes is either radiative or non-radiative. By studying the temperature dependance of the PL, a direct relationship may be found linking temperature and the dominant recombination process type. A simple study of the intensity of the PL allows the determination of material quality, as material with a high localised defect content are associated with a high incidence of nonradiative recombination and hence a low intensity output, and low material quality.

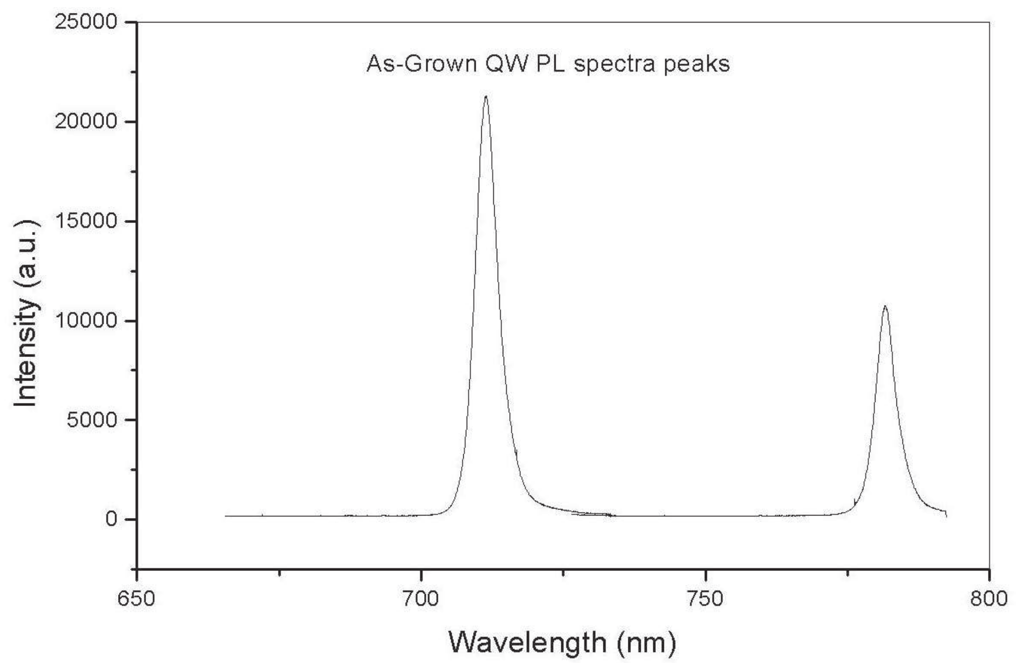

Figure 3.5: A typical PL experimental result spectra showing energy peaks corresponding to the ground state energy of as-grown QW's in the sample.

Chapter 4

The GaAs/AlGaAs QW System Results and Discussion

QW Intermixing studies were carried out on the unstrained GaAs/AlGaAs QW system. This chapter presents the experimental results obtained from these studies and a discussion of the findings.

4.1 Experimental

As discussed in Chapter 2, the QW structures used in this study were grown using the method of MOCVD growth. The GaAs/AlGaAs QW structures were grown on semi-insulating (100) GaAs substrates and consisted of (from the GaAs substrate up) a buffer layer of thickness 0.5μm, 100nm $Al_{0.54}Ga_{0.46}As$ barrier, 7nm GaAs QW, 100nm $Al_{0.54}Ga_{0.46}As$ barrier, 3nm GaAs QW, 100nm $Al_{0.54}Ga_{0.46}As$ barrier and 50nm GaAs capping layer to prevent oxidation of the AlGaAs layer. All layers were grown at 750^0C and were undoped to minimise dopant enhanced intermixing and built-in electric field effects that would complicate result interpretation. The thickness of the barrier layers ensured that the overlapping of electron wave functions from the finite energy barrier QW's that penerate a small distance into the barriers was essentially zero (the effect becomes negligible beyond 10nm)

After material growth, implantation of 25keV H, 100keV B or 650keV As was carried out using a variety of implantation doses (H dose range 5×10^{14} to $1 \times 10^{16} cm^{-2}$, B dose range 1×10^{13} to $2 \times 10^{14} cm^{-2}$, As dose range 7.1×10^{11} to $1.4 \times 10^{13} cm^{-2}$), at a variety of temperatures (liquid N_2 (LN_2) temperature, room temperature (RT), 100^0C, 200^0C and 300^0C). The samples were tilted with respect to the ion beam axis by 7^0 to minimise the effect of channeling. The ion energies and doses were chosen such that the damage profiles for each ion species covered both QW's with similar defect densities among the different implants as calculated by TRIM and shown in figure 4.1. The calculations showed that the collisional displacement density caused by As was about 700 times higher than that of H and about 15 times that of B, hence the doses implanted were scaled so that those of As were 700 times less than for H and 15 times less than for B. This allowed for comparison between intermixing results from different ion species. During implantation, part of the sample was masked to provide an unimplanted reference sample.

The samples were then annealed face down on a piece of fresh GaAs under Ar flow, (to prevent excessive loss of As from the surface of the material) using a rapid thermal annealer at 900^0C for 30s. This temperature was chosen as it has been shown to be the optimum

temperature for inducing intermixing and for material recover[15]. This was followed by low temperature (12K) PL, carried out at the University of New South Wales' Department of Condensed Matter Physics, using an Ar ion laser (514.5nm) as the excitation source. The luminescence was collected through a monochromator by a silicon photodetector.

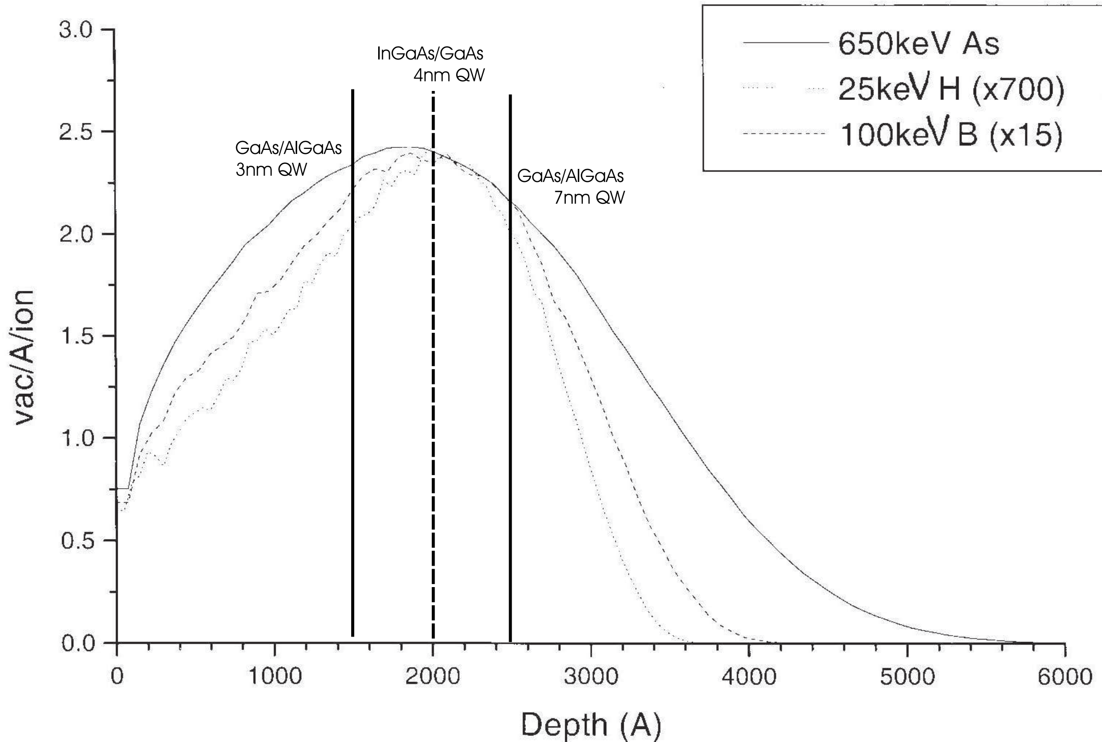

Figure 4.1: TRIM damage profile simulation with the position of the three QWs studied shown.

4.2 Results

4.2.1 *Experimental*

The implantation of Hydrogen and Arsenic was done in order to reconfirm previous experimental result trends for dose dependent and temperature dependent implantation in GaAs/AlGaAs QWs. Boron implantation was carried out to investigate the results for medium mass ion implantation and how these results compare with those gained for low and high mass ions. The 12K PLS dose dependent implantation results are shown in figures 4.2, 4.3and 4.4.

Displayed are the QW peaks from each of the four implantation doses for both QW's as well as comparison reference samples which were unimplanted and annealed. The peaks of the reference samples correspond to those from the as-grown samples (unimplanted and unannealed) showing that annealing alone does not result in intermixing of the QW's in this case. For dose dependent implantation, all implants were carried out at room temperature. The first set of peaks between 630 to 720 nm are emissions from the 3nm QW, and the second set of emission peaks from 740 to 800 nm correspond to the 7 nm QW. In figure 4.2, it is clearly observed that after implantation with $5 \times 10^{14} cm^{-2}$ H the emission wavelengths from both QW's are shifted to shorter wavelengths compared

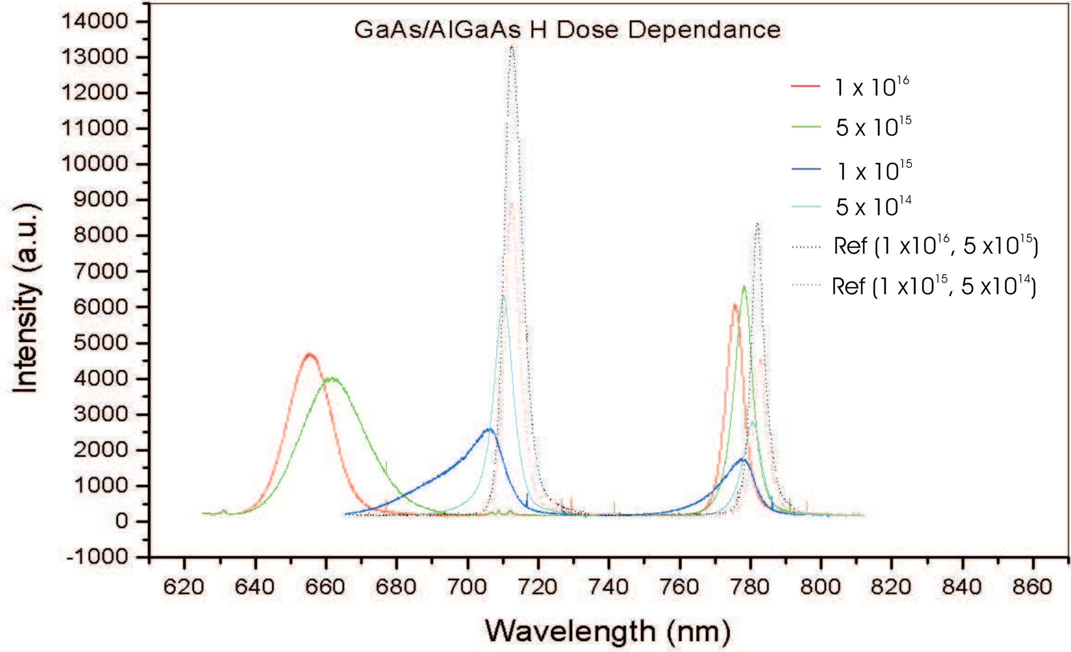

Figure 4.2: 12K PL spectra for H implanted GaAs/AlGaAs

with the unimplanted and annealed reference samples. As implantation dose is increased, the resulting emissions show an increase in blue shift. This also occurs for the As dose dependent implantation, where the 7.1 $\times 10^{11} cm^{-2}$, annealed samples show a wavelength blue shift with respect to the reference samples in both QW's, and an increase in dose shows a corresponding increase in blue shift (figure 4.4). The Boron implantation results (figure 4.3) show a smaller shift despite scaling doses to create a similar amount of damage as in the case of H and As implantation. This result is explored in the discussion section. Plots of energy shift (of QW emission peaks with respect to reference peaks) as a function of implantation dose for each ion species are displayed in figures 4.5, 4.6, 4.7.

Temperature dependent implantation was also carried out with H, B and As ions. In each case one of the intermediate doses was selected and kept constant while the implantation temperature was varied. The PLS results for these are shown in figures 4.11, 4.15 and 4.12, and corresponding energy shift with implantation temperature plots (with respect to unimplanted and annealed reference samples) are shown in figures 4.13, 4.16 and 4.14. It can be seen immediately that the difference in shift with temperature of implantation does not show as large a dependence as the previous results did on dose change.

Errors in the measurements result from small growth variations across the sample and amount to about $\pm$ 5meV error.

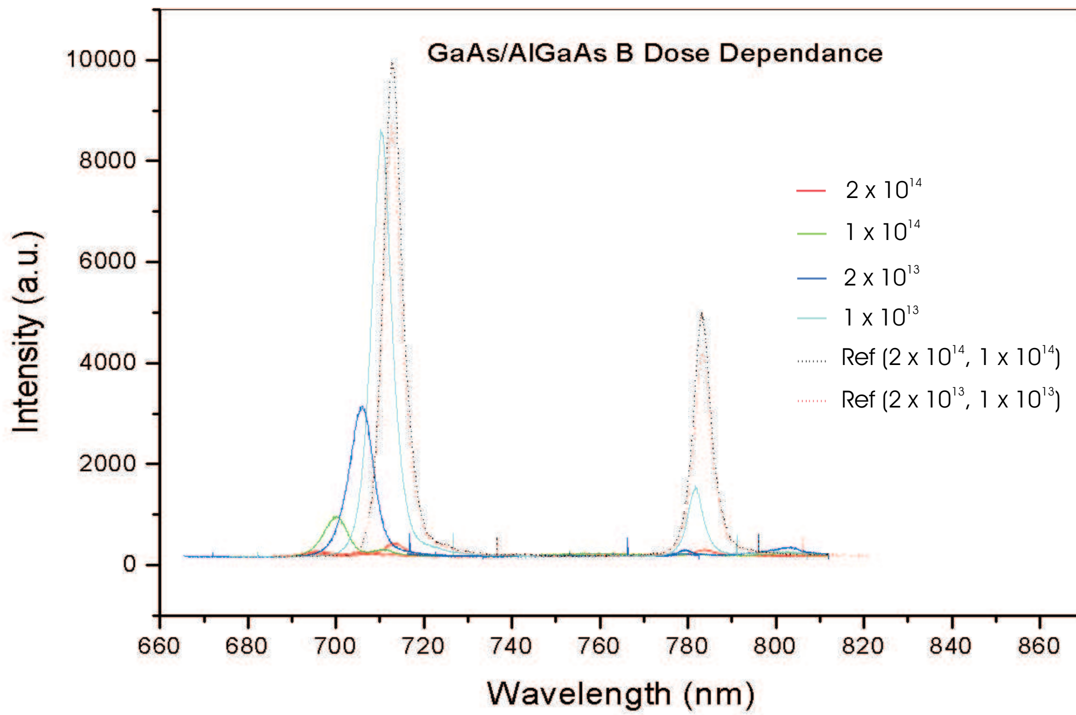

Figure 4.3: 12K PL spectra for B implanted GaAs/AlGaAs

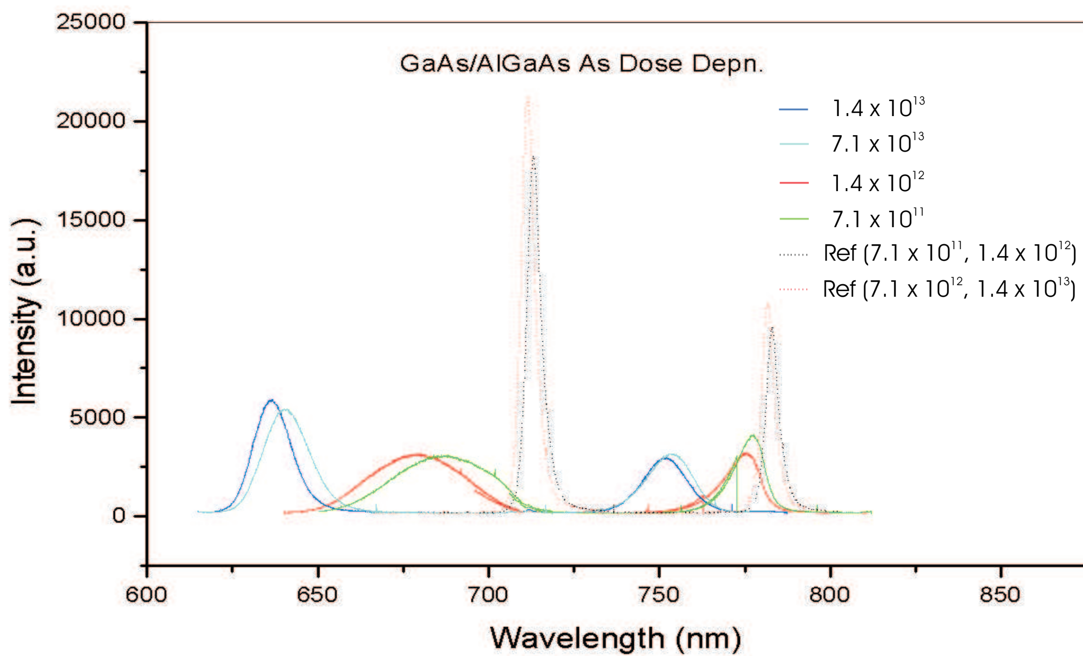

Figure 4.4: 12K PL spectra for As implanted GaAs/AlGaAs

4.3 Discussion

Previous studies of H and As implantation into GaAs/AlGaAs QW systems have shown that strong relationships between implantation parameters and the extent of QWI seen in the PLS emissions exist[15],[14]. The results presented above reconfirm these relationships. Boron implantation into the GaAs/AlGaAs QW system has also been investigated, and the results are discussed below.

4.3.1 *Dose dependence*

The increase in energy shift seen with increase in implantation dose is consistent with previous results. For both light (H) and heavy (As) ion species, an increase in implanted dose results in an increase in QWI, seen as in figure. Reasonable intensity recovery is also seen for the QW's in the PL spectra, and although the intensity is measured in arbitrary units (a.u.) comparison between spectra is possible since each measurement was taken under the same conditions, on the same optical set up, using the same detector. The recovery of intensity indicates that the post implantation annealing is effective in removing most of the extended defects that act as non-radiative recombination centers, reducing the intensity of the PL.

Although the shifts obtained for both H and As dose dependent implantation show significant blue shifting in both cases, the mechanisms responsible for this blue shifting are quite different for low and high mass ion species.

Low mass ion implantation results in dilute damage cascades and the formation of a large number of point defects compared to extended defects or point defect clusters[24]. Post

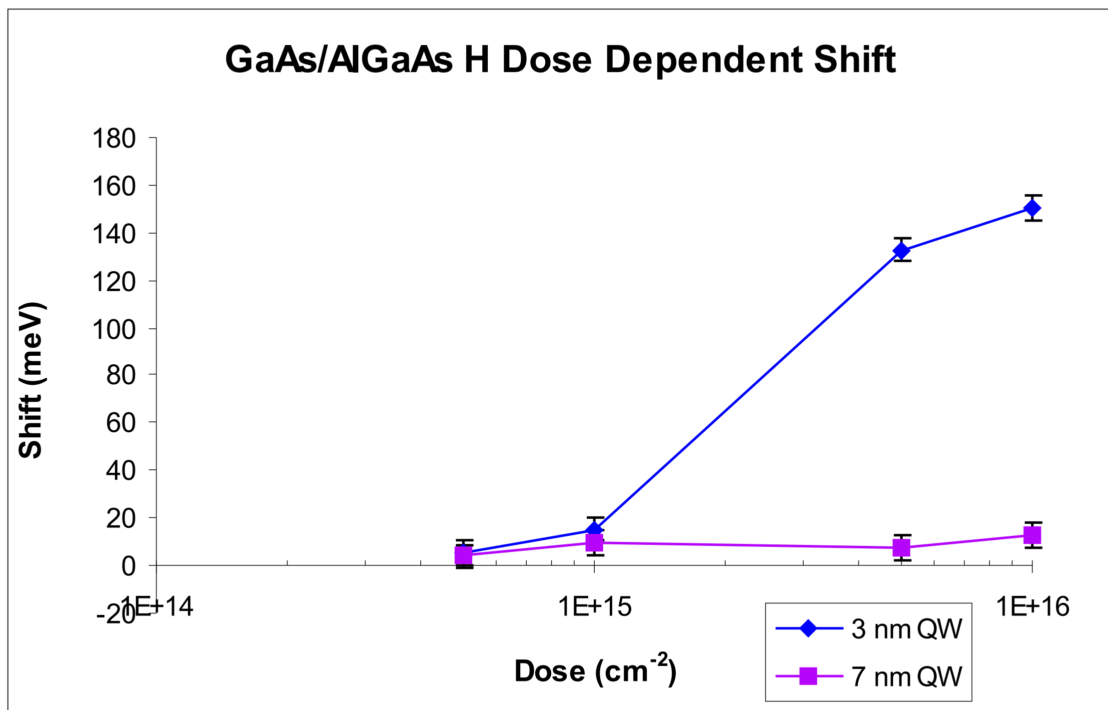

Figure 4.5: Implantation energy shift as a function of dose for H

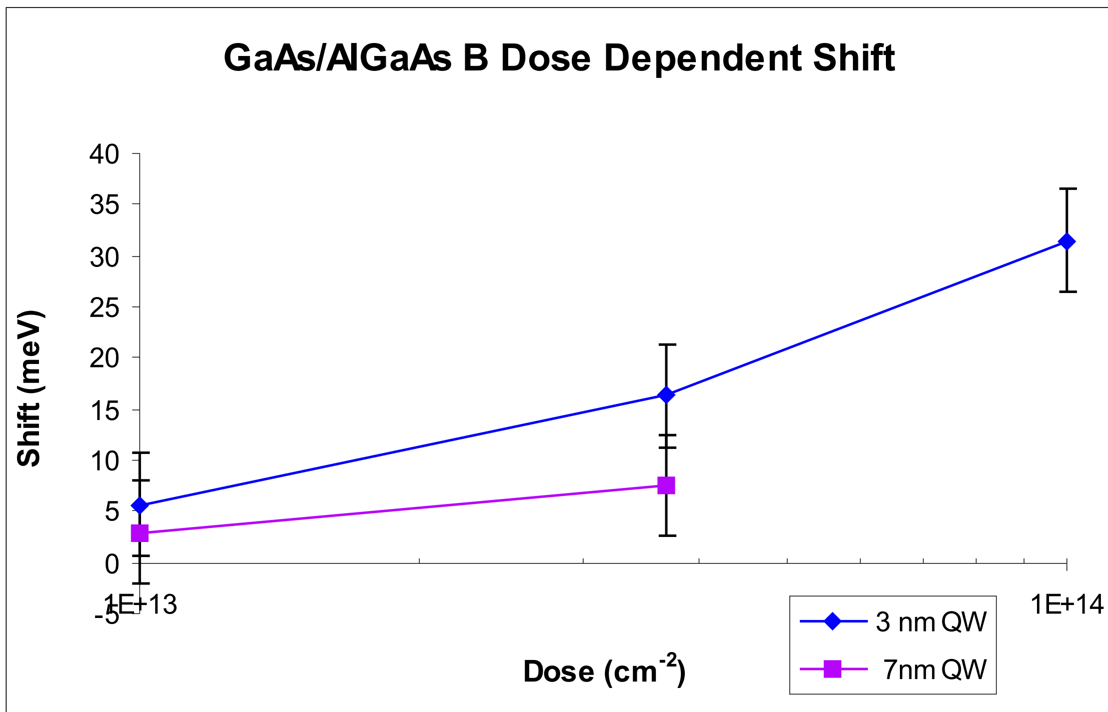

Figure 4.6: Implantation energy shift as a function of dose for B

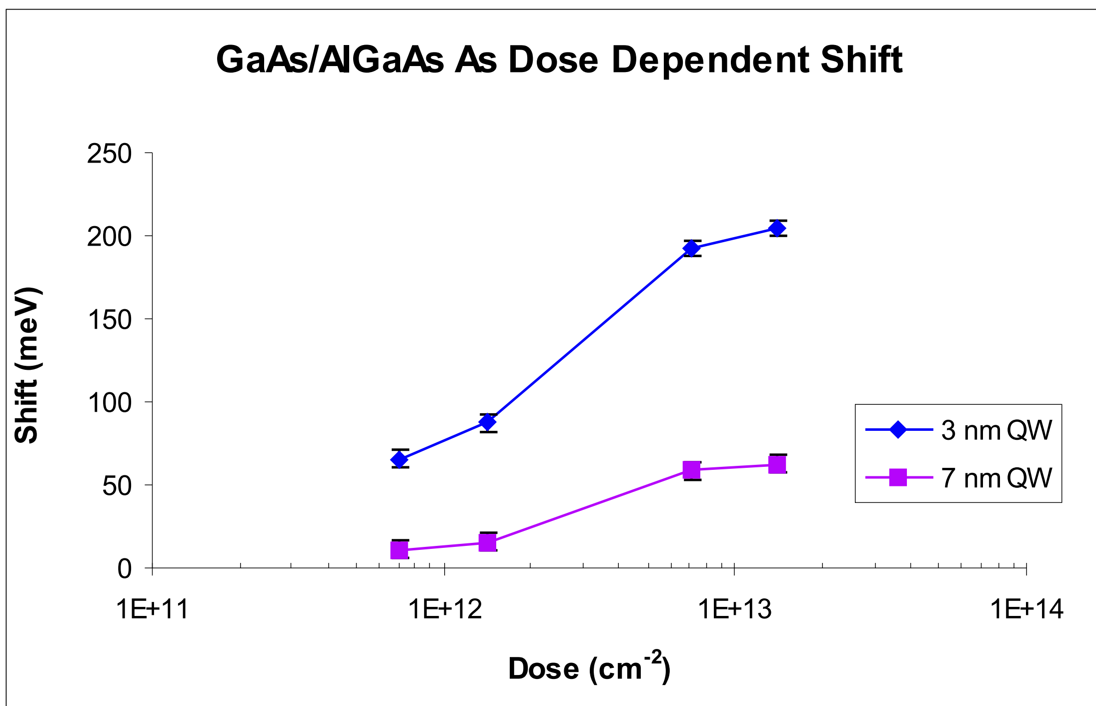

Figure 4.7: Implantation energy shift as a function of dose for As

implantation annealing allows the large number of point defects generated during the implantation to migrate across the QW layers producing an intermixed system. Thus it is easy to see how simply increasing the implantation dose results in a larger number of point defects avaliable for intermixing and a subsequent increase in intermixing and observed blue shift in the PL spectra. It would be expected that as dose continues to increase, a saturation effect would be observed in the number of point defects created, beyond which the number of point defects would be so great that they would begin to recombine and simply increasing the dose further would not result in any increase in intermixing, however this effect was not observed in my results or in previous work, indicating that much higher doses are required for this effect to be seen[25].

High mass ion implantation however does not result in the same number of point defects created during the implantation process. Rather a large number of extend defects and point defect clusters are formed. During post implantation annealing, the thermal energy imparted to the point defect clusters breaks them up, resulting in a large number of point defects avaliable for diffusion. The annealing step also recovers the material, removing a large number of the extended defects formed, reducing the number of non-radiative recombination centers in the material and producing an observable intermixing shift of comparable magnitude to that observed in the low mass ion implantation case. An increase in implantation dose results in an increase in the number of point defect clusters and an increase in the number of point defects avaliable for diffusion. As dose is increased for high mass ions, the number of extended defects formed increases also. This results in a degradation of material quality as not all of these are able to be removed by annealing, and for higher and higher doses, excessive thermal treatment would be necessary in trying to recover the material. This would result in a drop in PL intensity, thus careful consideration to dose must be given in the use of high mass implanted material for optoelectronic device application to ensure that an acceptable emission level is obtained.

When heavy and light mass ion implantation energy shift is compared, it may be seen that at low doses heavier ions are more effective at inducing intermixing due to their ability to produce more damage in the material compared to the dilute defect cascades of the light ions. However at high doses, a saturation effect is seen in the amount of intermixing occuring in the heavy ion implants. Thus at higher doses, the low mass ions, that do not give a shift saturation, are more effective at inducing intermixing than the high mass ions. This exemplifies the fundamentally different nature of defects caused by high and low mass ion implantation.

Another important result observed in the dose dependent implantation energy shift results, is the relative shift between the two QW's. In both the H and As implantation case (very prominent in the H case), the 3 nm QW experiences a larger energy shift for each dose than the 7 nm QW, despite similar defect concentrations across both QW regions. This shows an intermixing dependence on QW size. A similar effect was observed in previous work [15] and is best explained with reference to figure 4.8. For thin wells the ground state electron energy lies close to the barrier energy levels for both conduction and valence band. Although a small perturbation in well shape is expected to create a large change in energy level, the energy level is so close to that of the barriers that there is little room for movement of the energy levels and the resulting PL spectrum shift is low. For a wide well a small change in well shape results only in a small change in energy level due simply to the width of the well (continuum limit). Intermediate wells initially have their ground

state energy at a lower level compared with the barriers, thus the energy level has a larger range of energies between which it can move, and responds better to small pertubations in well shape.

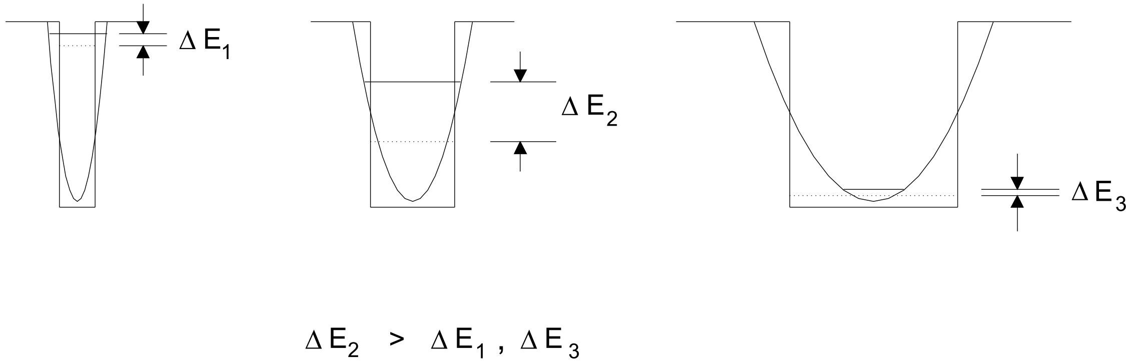

$\Delta E_2 > \Delta E_1 , \Delta E_3$

Figure 4.8: Schematic showing the effects of well width on shifting levels.

As demonstrated above, the intermixing mechanisms for high and low mass ions are fundamentally different. Boron implantation was carried out in order to investigate a medium mass ion to see which if either intermixing process is favoured, and to see if there are any links between the high and low mass ion intermixing mechanisms. Boron was specifically chosen as it is a group III element and so is chemically and electronically similar to the group III material constituents that provide the point defects for intermixing.

It was hypothesised that a medium mass ion would show similar intermixing mechanisms to those of the high mass ion. It was expected that the formation of point defect clusters and extended defects would be favoured over the formation of point defects, although the point defect clusters were not expected to be as large as those created by high ion mass implantation and the extended defect concentration not as high due to a lower ion mass. The resulting PL spectrum was expected to show good recovery of PL intensity due to the lower concentration of extended defects expected from B implantation, which would be removed by annealing. It was also expected to show good energy shifts as the smaller point defect clusters were broken up resulting in many point defects avaliable for diffusion. The dose dependent B PL spectrum and shift graphs are displayed in figures 4.3 and 4.6. The results obtained from the PL spectrum were not at all what was expected! As can be seen only a slight blue shifting with increase in implantation dose is observed for the 3nm QW, while only the lowest doses resolved a clear second 7nm QW peak. This result was very surprising. Instead of giving good shifts the intermixing was highly surpressed. A number of postulates were formed to explain this result.

The first thing to consider before any physical explanations are possible is whether any step of the fabrication or manipulation processes might be causing the supression. The MOCVD growth is a very reliable QW fabrication method, however there was the remote possiblity of impurity incorporation from the substrate during the manipulation processes. To remove this possibility, the QW heterostructure was regrown with AlAs/GaAs superlattice layers above the GaAs buffer layer and before the QW layers, to trap any defects that may migrate into the active regions from the substrate during processing. The resulting PL spectrum from the as-grown QWs showed two QW peaks with good intensity, suggesting excellent quality QWs.

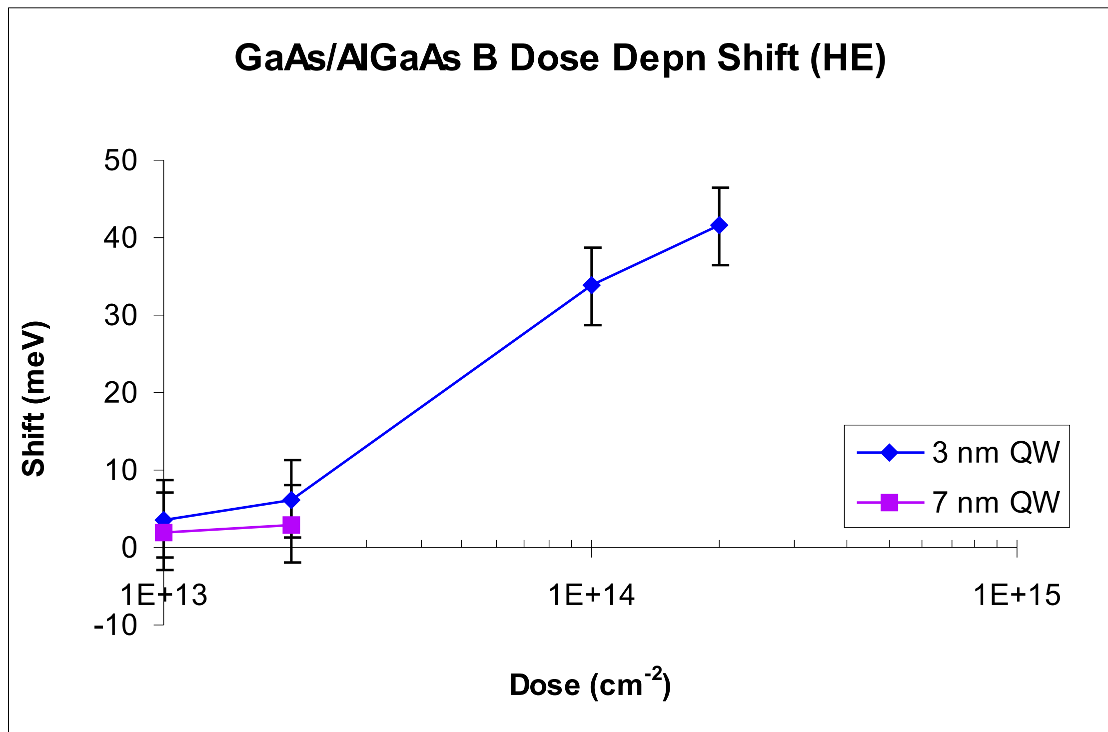

Figure 4.9: Repeated results for implantation energy shift as a function of dose for B - High Energy implanter

There was also the possibility that the implantation doses had been incorrect. This could have occured if the vacuum in the implanter degrades, resulting in neutralisation of some of the ion beam. These neutral components would still be implanted but would not be recorded by the current integrater so a different dose would be implanted. A different dose would result in a different defect density concentration through the QW regions than that obtained for the H and As implantation, thus although intermixing occured for the B samples, the relative energy shifts between the different ion implants could not be compared, and the B results would appear very different to the other ions.

In order to counter for this effect, the B implantation on the new samples was carried out on the high energy implanter used for the As implantation. This had not been done for the first lot of implants, because implanting at 100keV on the high energy implanter is near the lower limit of its implantation range, and the low energy implanter used was much more suitable for this energy range. The samples were thoroughly cleaned after each processing step using trichloroethelyne as a degreaser, followed by acetone, and then methanol to ensure a clean surface prior to annealing. The annealing was carried out on fresh pieces of material from the same sample growth to minimise impurity inclusion in this step. Following these rigorous experimental processing steps, 77K PL was carried out on the samples.
The energy shift graph is displayed in figure 4.9. Once again a small energy shift with increase in dose is observed!

At this stage it was certain that all experimental effects had been removed, and the observed supression was resulting from some physical or chemical mechanism.

A low level of intermixing is indicative of a low number of point defects in the active region of the QW. Two hypothetical mechanisms have been suggested to explain the low intermixing result.

The first possibility is that Boron is binding with the point defects it creates in the material during implantation. This would directly remove point defects from the system, reducing the number avaliable for intermixing, and lowering the observed shift. If the complexes formed were also thermally stable, they would not be broken up during post implantation annealing, and higher temperature anneals would be needed to release the point defects and increase the intermixing again. This suggestion was further tested by reannealing the Boron dose dependent samples at 950^0C for 60s. A longer, hotter anneal would make the point defect - B clusters that were less thermally stable break up, releasing point defects into the system, resulting in an observed increase in blue shift in the PLS spectrum. The results from this work are shown in figure 4.10.

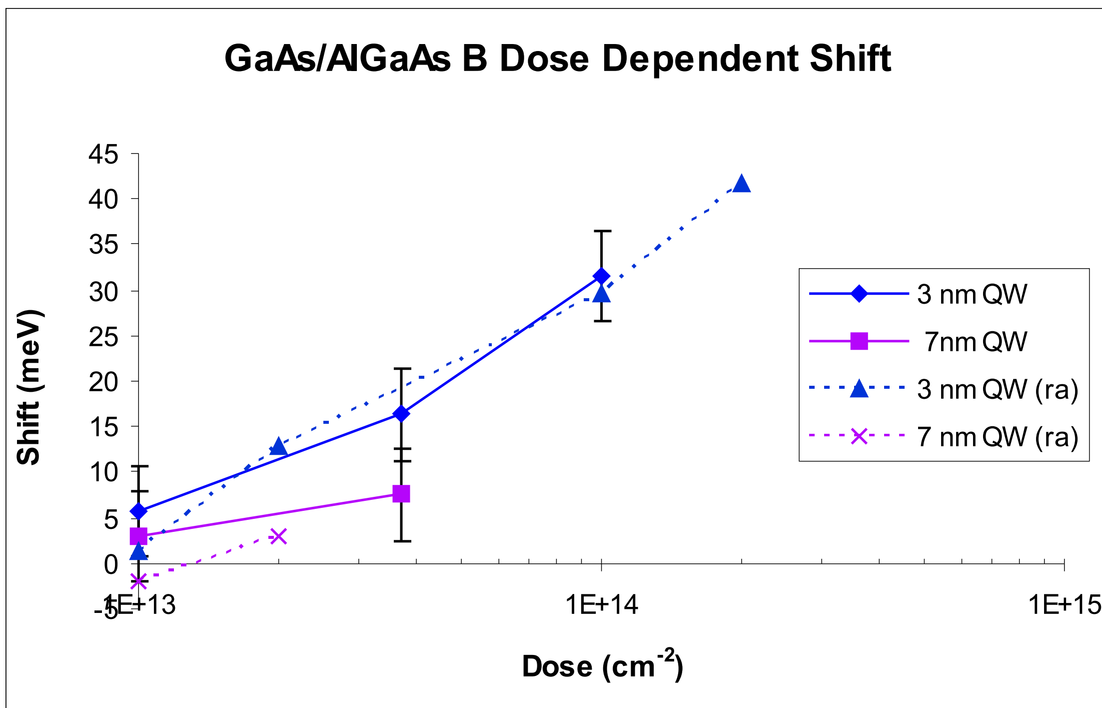

Figure 4.10: B implanted GaAs/AlGaAs dose dependent shift results; reannealed (ra) at 950^0C for 60s

The results showed no major changes in shift, thus no conclusions can be drawn about the nature of the mechanisms involved in the lack of shifting. The lack of shift doesn't disprove the point defect - B cluster hypothesis, because the point defects released on the break up of clusters could still be thermally stable at 950^0C resulting in no observed shift increase. Further investigations would focus on implantation of other medium mass ions to compare their intermixing shifts to those of B. It would be beneficial to study ions such as Carbon (also chemically stable, and close to B) and Aluminium (another lattice constituent, but still with a mass number significantly smaller than As) to see the similarities and differences in results. For example, if the results from C were significantly different to those of B, it would indicate a lattice interaction such as B sitting in Ga

vacancies resulting in strain related shifts, however if the results were similar, it would indicate a real medium mass ion effect.

The second postulate comes from the fact that Boron is a group III element. This was a deliberate choice to reduce the possibility of chemical reactions occuring in the system and has been successfully applied to the implantation of As and Ga, also group III elements[14],[15],[26]. The possibility in this case however, is that Boron has been incorporated into the lattice structure by sitting in place of Gallium vacancies produced during the implantation. Since Boron is a much smaller ion than any of the lattice constituents this could result in a strain effect in the system, that when annealed could lead to red shifting that would counteract the blue shifting effect of the point defect diffusion, leading overall to a lower energy shift. Once again further study is required with different mass ions as described previously in order to determine whether this effect is significant.

4.3.2 *Temperature Dependence*

Previous results have shown that energy shift dependence on temperature is a much smaller effect than that observed in the dose dependence results[14],[15]. The H and As temperature dependence shift results are displayed in figures 4.13 and 4.14.

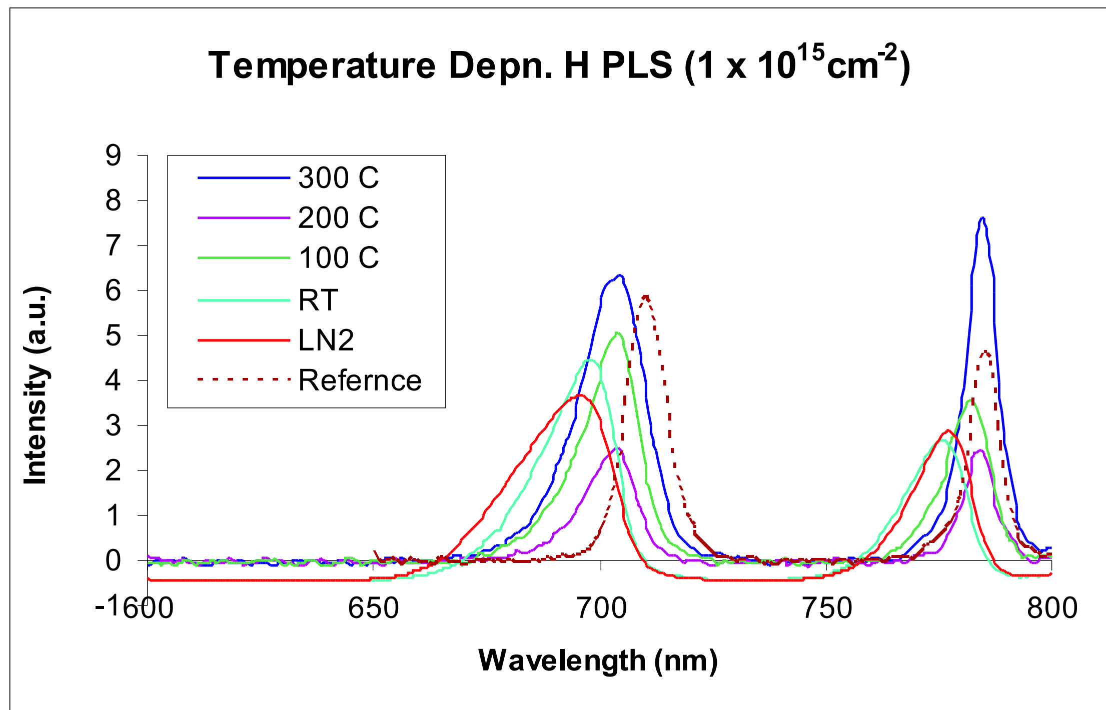

Figure 4.11: 77K PL spectra for H temperature dependent GaAs/AlGaAs

Low mass ion implantation displays a decrease in energy shift with an increase in implantation temperature and is characterised by the formation of large numbers of point defects. If the implantation temperature is high, then some of the thermal energy is imparted to the point defects created during implantation causing them to annihilate one another, for example an interstitial defect may recombine with a vacancy. This process is known as *dynamic annealing*. This effect is also observed strongly in AlGaAs[15]. An increase in

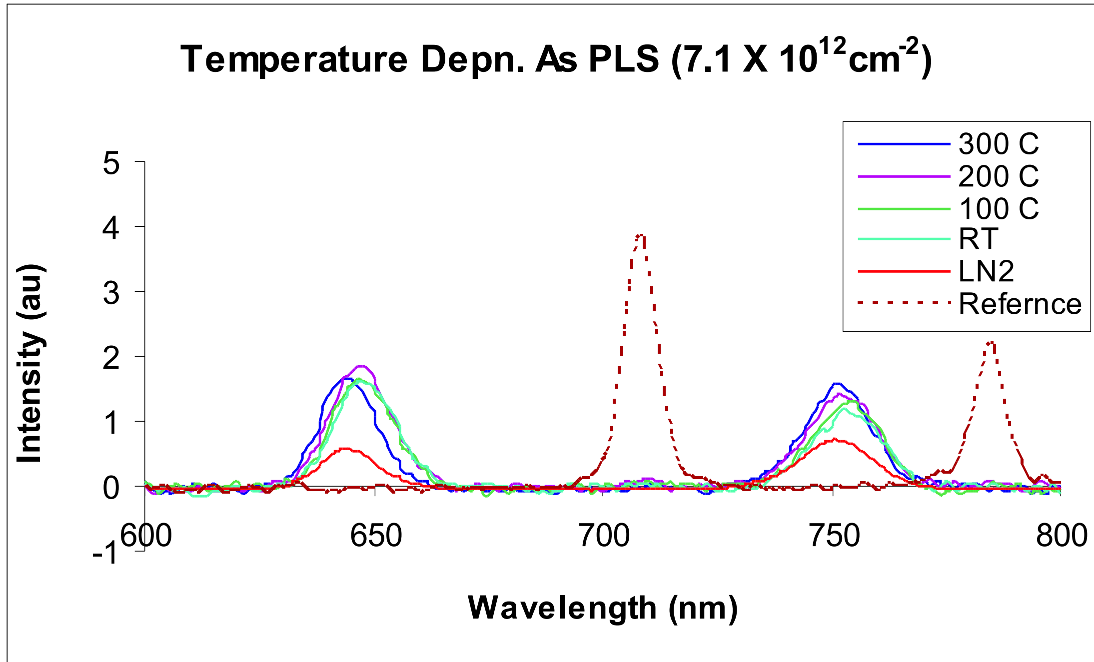

Figure 4.12: 77K PL spectra for As temperature dependent GaAs/AlGaAs

implantation temperature results in an increase in the amount of dynamic annealing, resulting in fewer point defects being avaliable for intermixing than at lower temperatures, thus the observed energy shift decreases with an increase in implantation temperature. This result agrees with previous low mass ion implantation results[15].

High mass ion implantation however displays a different trend. It was expected that an increase in implantation temperature would result in an increase in the degree of intermixing. As the temperature increased, more dissociation of the large defect clusters formed during implantation would occur. This would result in a larger number of point defects avaliable for intermixing and a corresponding increase in the energy shift with temperature. However the results showed only a slight increase in energy shift with temperature increase. It must therefore be summarised that the large defect clusters were more thermally stable than first thought and were not as affected by the increase in temperature as expected. Thus one would have to go to higher implantation temperatures in order to observe a more pronounced effect. This result also agrees with that found previously for high mass implantation[15].

The study of Boron temperature dependent implantation aimed to investigate the effect of temperature on the smaller damage clusters created by medium mass ion implantation. The temperature dependent shifts for Boron are shown in figure. Very little temperature dependent shift was observed (figures 4.15 and 4.16)
It had been expected that if smaller defect clusters were being formed during medium mass ion implantation compared with those formed during high mass ion implantation, then they would have a lower thermal stability than their larger counterparts and would be affected more easily by temperature increase. This however was not observed. It is concluded that there is a competing effect between the breaking up of defect clusters (releasing point defects into the system) and dynamic annealing effects (resulting in the annihilation

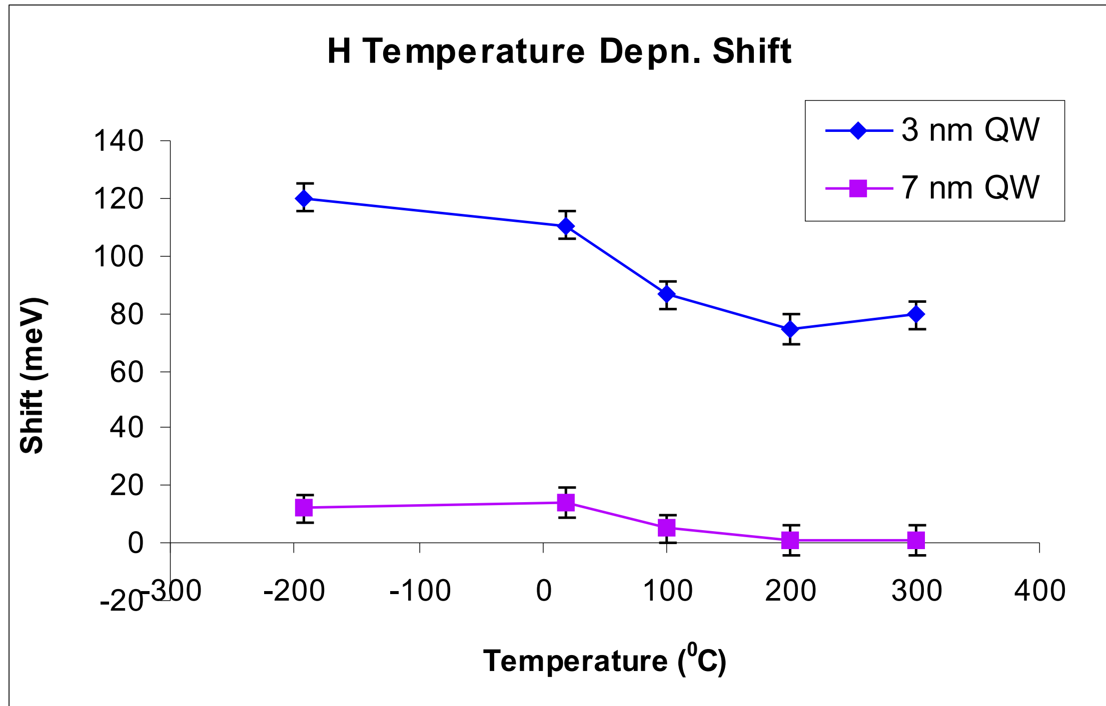

Figure 4.13: Implantation energy shift as a function of temperature for H

of point defects) resulting overall in a low residual point defect population avaliable for intermixing. It would be interesting to study the temperature dependent shift effects of another medium mass ion such as Al, where the mass is slightly higher, to determine the extent of this effect. Although temperature has not been found to be a parameter that could be varied to create larger energy shifts, the lack of temperature induced variation is a positive factor in that it shows that thermal stability during implantation processing is not a large issue, and small temperature variations during implantation are tolerable while other precise effects are being created (for example in the fabrication of a monolithic integrated chip that requires different implants on different parts of the sample).

The investigations carried out on intermixing in the unstrained GaAs/$Al_xGa_{1-x}As$ QW system have demonstrated the importance of this system with regards to optoelectronics applications. Further study is warranted on medium mass ion implantation by using other ion species, for example C and Al, in order to complete the understanding of the medium mass ion intermixing mechanisms.

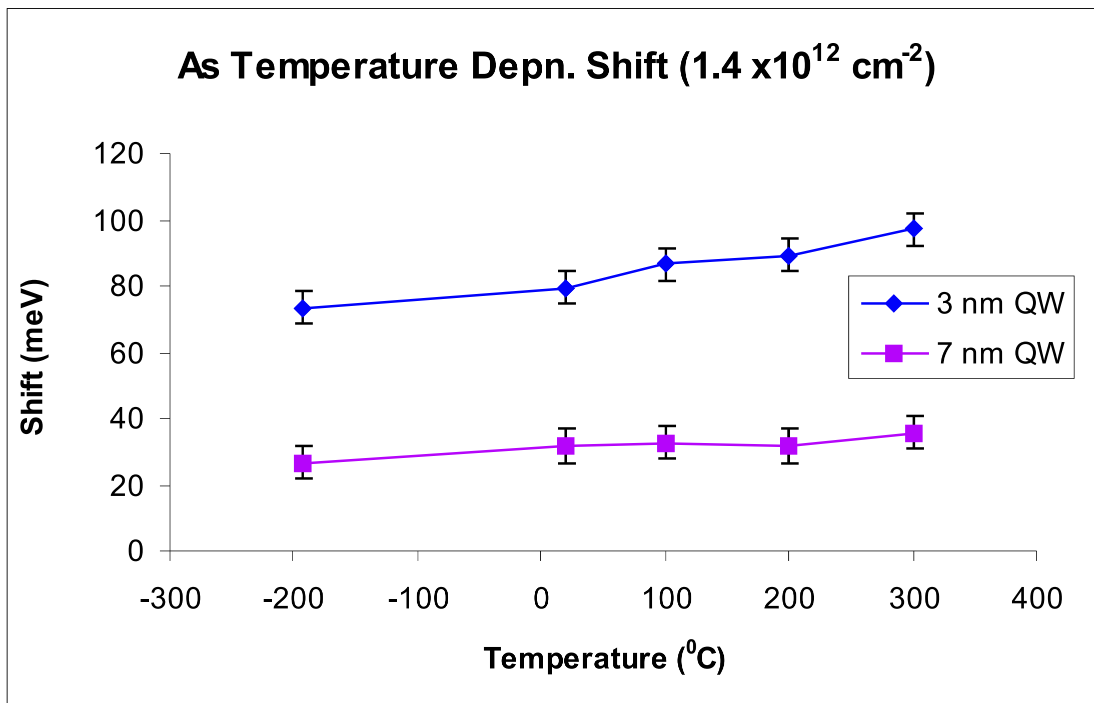

Figure 4.14: Implantation energy shift as a function of temperature for As

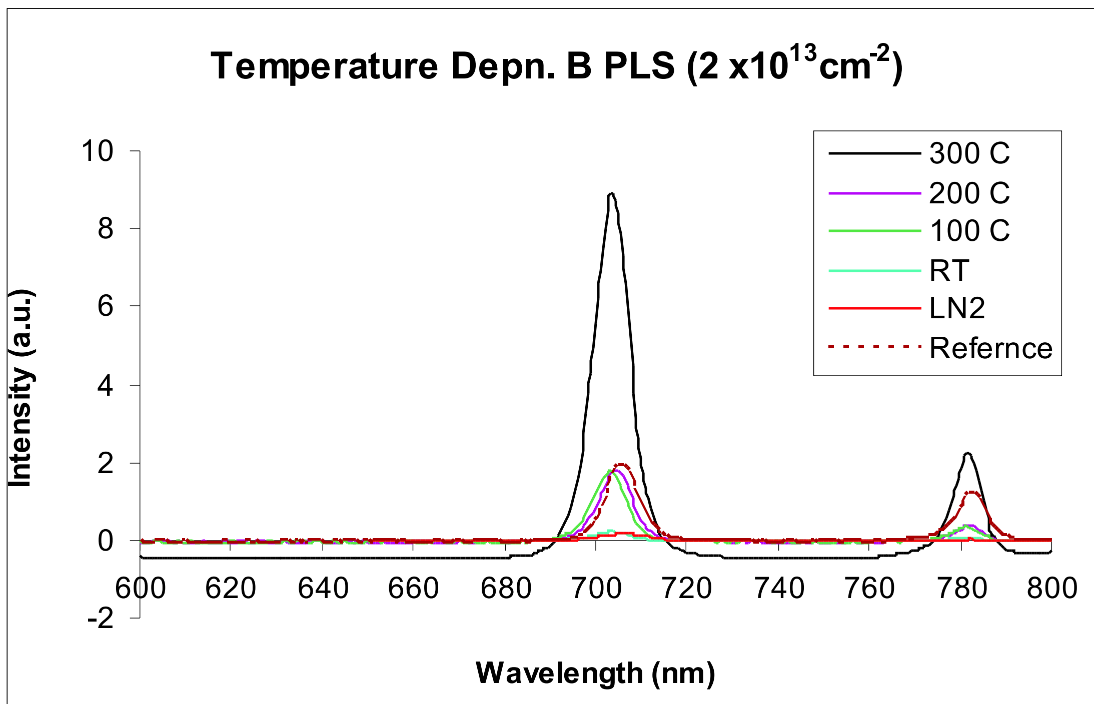

Figure 4.15: 77K PL spectra for B temperature dependent GaAs/AlGaAs

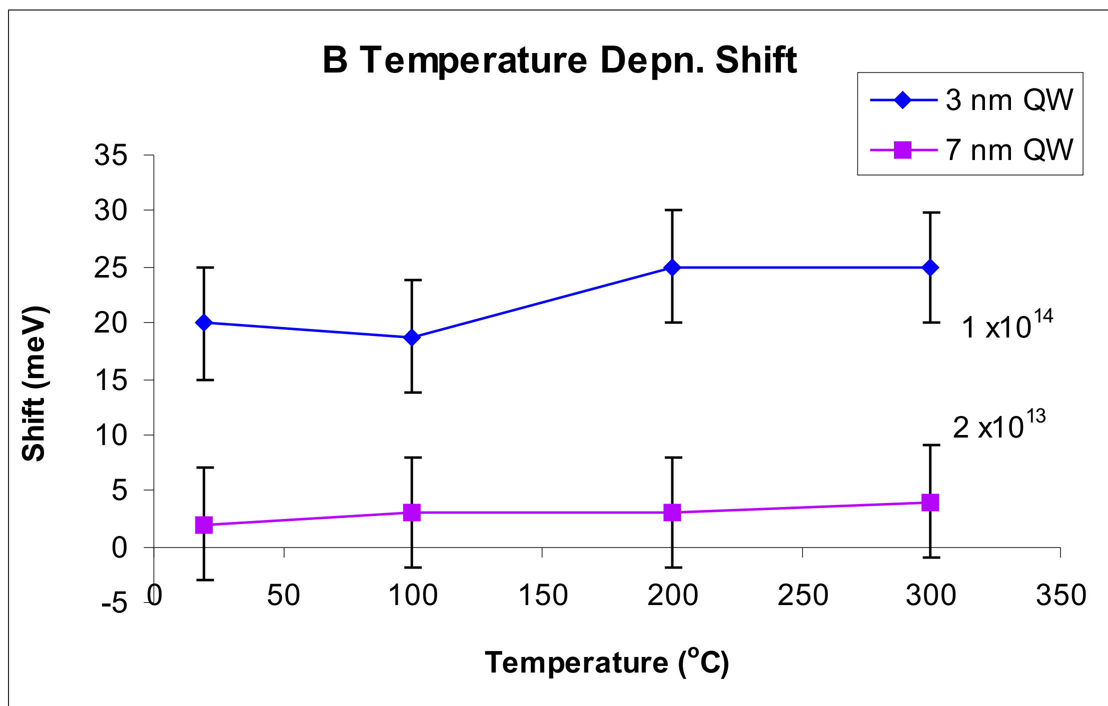

Figure 4.16: Implantation energy shift as a function of temperature for B

Chapter 5

The InGaAs/GaAs QW System Results and Discussion

Preliminary QW Intermixing studies were carried out on the strained InGaAs/GaAs QW system. This chapter presents the experimental results obtained from these studies and a discussion of the findings.

5.1 Experimental

As previously, MOCVD growth was employed as the QW fabrication process. The InGaAs/GaAs QW structures were grown on semi-insulating (100) GaAs substrates and consisted of (from the GaAs substrate up) a buffer layer of thickness 0.4 μm, 100nm GaAs barrier, 4nm $In_xGa_{1-x}As$ QW and 200nm GaAs barrier/capping layer. The subscript x indicates the percentage of each group three element in the material. The quantum wells were grown with $x = 0.3$ or 0.5. All layers were grown at 650^0C and were undoped to minimise dopant enhanced intermixing and built-in electric fields that would complicate result interpretation.
After material growth, implantation of 25keV H, 100keV B or 650keV As were carried out using a variety of implantation doses (H dose range 5×10^{14} to $1 \times 10^{16} cm^{-2}$, B dose range 1×10^{13} to $2 \times 10^{14} cm^{-2}$, As dose range 7.1×10^{11} to $1.4 \times 10^{13} cm^{-2}$), at room temperature (RT). The samples were tilted with respect to the ion beam axis by 7^0 to minimise the effect of channeling. The same doses as for the GaAs/AlGaAs system were used to create similar damage profiles between ions so that result comparison could be made between the intermixing results of different ion species. During implantation, part of the sample was masked to provide an unimplanted reference sample.
The samples were then annealed face down on a piece of fresh GaAs under Ar flow, (to protect the surface of the material) using a rapid thermal annealer at 800^0C for 30s. This was followed by low temperature (77K) PL using a solid state (532nm) laser as the excitation source, the luminescence was collected through a monochromator by a germanium photodetector.

5.2 Results

5.2.1 *Experimental*

Unlike the unstrained GaAs/AlGaAs system, the effect of strain in the InGaAs/GaAs system means that simply annealing the sample will cause some intermixing effects due to strain effects and the lower thermal stability of In containing material. Thus annealing

temperature studies at 700^0C, 800^0C and 900^0C for 30s were carried out to determine the optimum annealing temperature, i.e. the highest temperature at which little annealing induced intermixing occurs for each of the In concentrations. A plot of shift vs. annealing temperature is shown in figure 5.1. As can be seen at temperatures up to 800^0C little annealing induced intermixing takes place for either of the In concentrations, but at 900^0C there is a large energy shift caused by the annealing, that increases with increasing In content. Hence 800^0C was chosen as the optimum annealing temperature for the $In_xGa_{1-x}As/GaAs$ QW system.

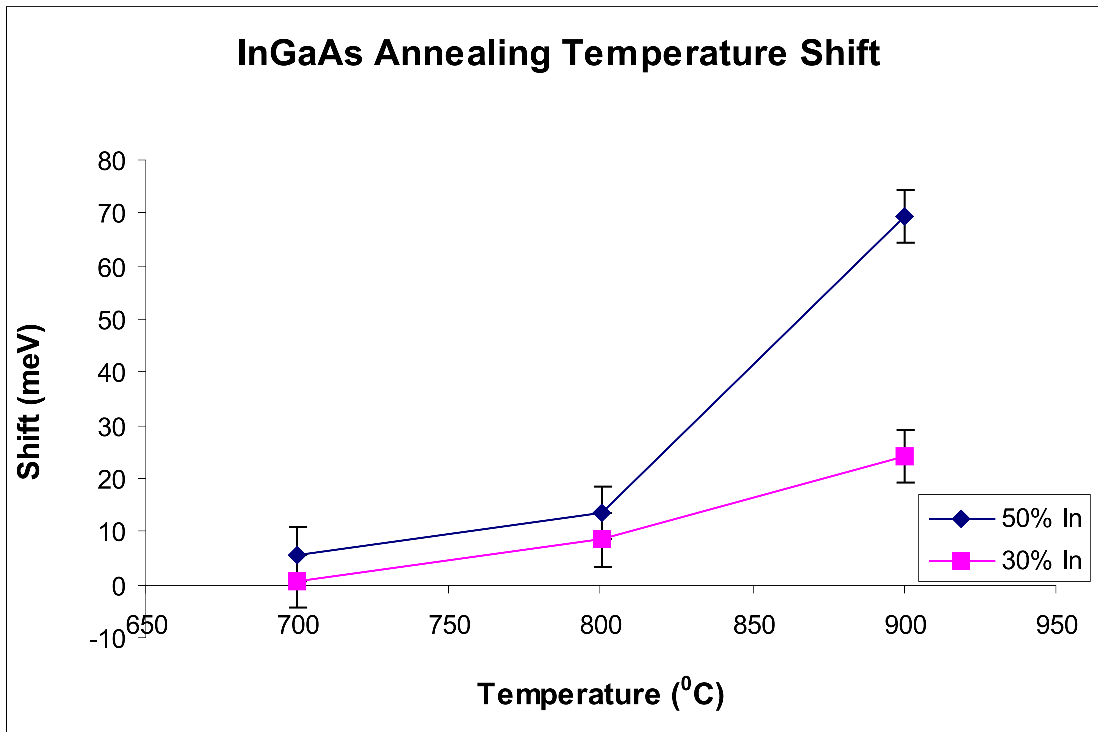

Figure 5.1: Annealing temperature study results for the $In_xGa_{1-x}As/GaAs$ QW system

The implantation of H, B and As was done in order to investigate the effect of ion mass on increasingly strained systems (increasing In content). The B shift results are shown in figure 5.2. For dose dependent implantation, all implants were carried out at room temperature. As discussed, the annealing temperature was chosen to cause as little annealing induced intermixing as possible. The preliminary results showed that the results for the $In_xGa_{1-x}As/GaAs$ QW system differ substantially from those gained from the GaAs/AlGaAs system, and that strain plays an important role in QW intermixing.

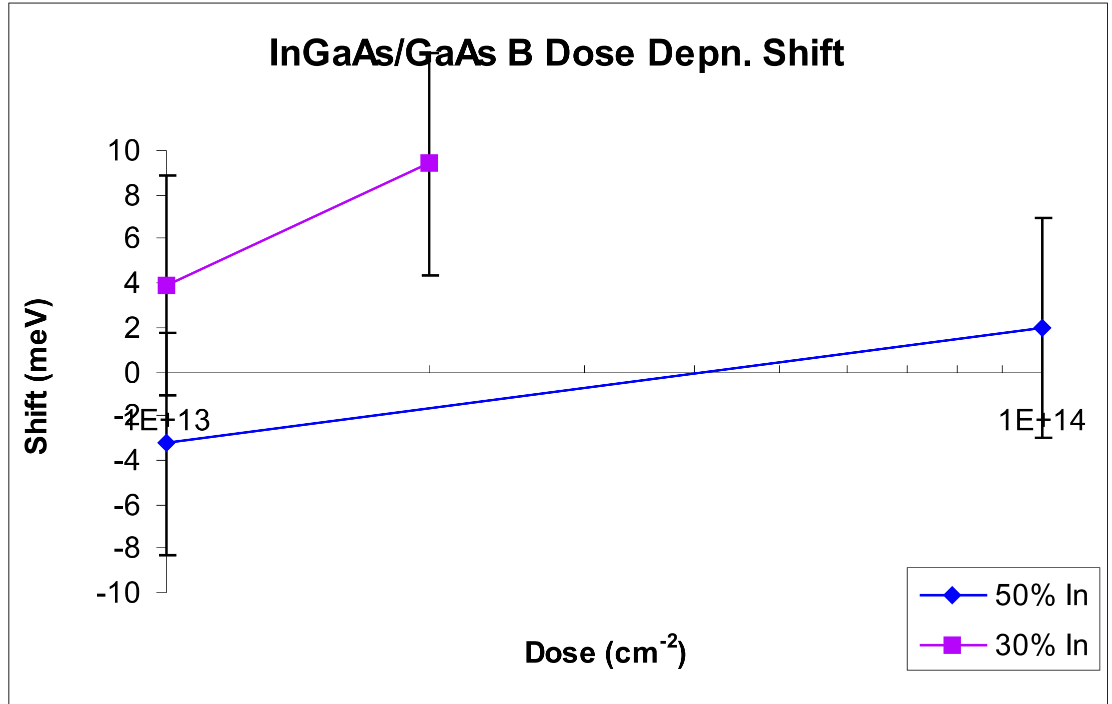

Figure 5.2: Dose dependent energy shift results for B implanted $In_xGa_{1-x}As/GaAs$ QW system

5.3 Discussion

Although only preliminary dose dependent implantation was carried out due to time constraints, interesting intermixing results were gained that warrant further investigation.

5.3.1 *Dose dependence*

Intermixing of the $In_xGa_{1-x}As/GaAs$ QW system is complicated by the presence of strain. In contrast to the GaAs/AlGaAs system where the lattice constants of the well and barrier materials differ by only 0.13% where as the uni cell of $In_xGa_{1-x}As$ can be as much as 3.6% larger ($x = 0.5$) than that of GaAs. The strain energy produced in the system must be elastically accomodated by the lattice and figure 5.3 demonstrates the effects of strain in a QW system. The resulting strain on the well section is due to both shortening parallel to the well/barrier interface (biaxial compression) and elongation normal to the well/barrier interface (uniaxial tension). The strain energy in the system is accomodated up to a certain critical thickness, beyond which it will result in threading dislocations in the material[27]. The dose dependent PLS results for H, B and As for both 30% and 50% In content were difficult to resolve and in most cases only resolution of the lower two doses was possible. This indicates that the annealing temperature is not high enough to recover the material's radiative properties sufficiently in higher dose cases where more damage has been caused. This is not surprising, as it has been shown that GaAs is more susceptible to ion beam damage than AlGaAs[15].
The resolved peaks for all three ions showed a reduction in energy shift over all doses compared with the results obtained from the unstrained GaAs/AlGaAs system. The Boron implantation results especially show how the effects of strain can influence the intermixing. The energy shift vs. dose graph revealed *both* blue *and* red shifting of the PL spectra.

The explanation for this comes from considering the strain in the QW layer. Compressive strain in the growth plane results in a widening of the bandgap energy (Figure 5.3). When the QW system is annealed, the system relaxes and the bandgap energy decreases, resulting in a red shift in the emitted luminescence. This effect directly competes with the blue shifting that results from diffusion of point defects, cancelling and resulting in a low observed energy shift. The Boron results support this theory with the 50% In results showing more tendency towards red shift than the 30% results as expected since the 50% system is more highly strained than the 30% system. An increase in implantation dose also shows an increase in blue shift as the effect of defect driven intermixing is stronger for higher implantation dose due to the higher concentrations of point defects avaliable for intermixing as discussed for the GaAs/AlGaAs system.

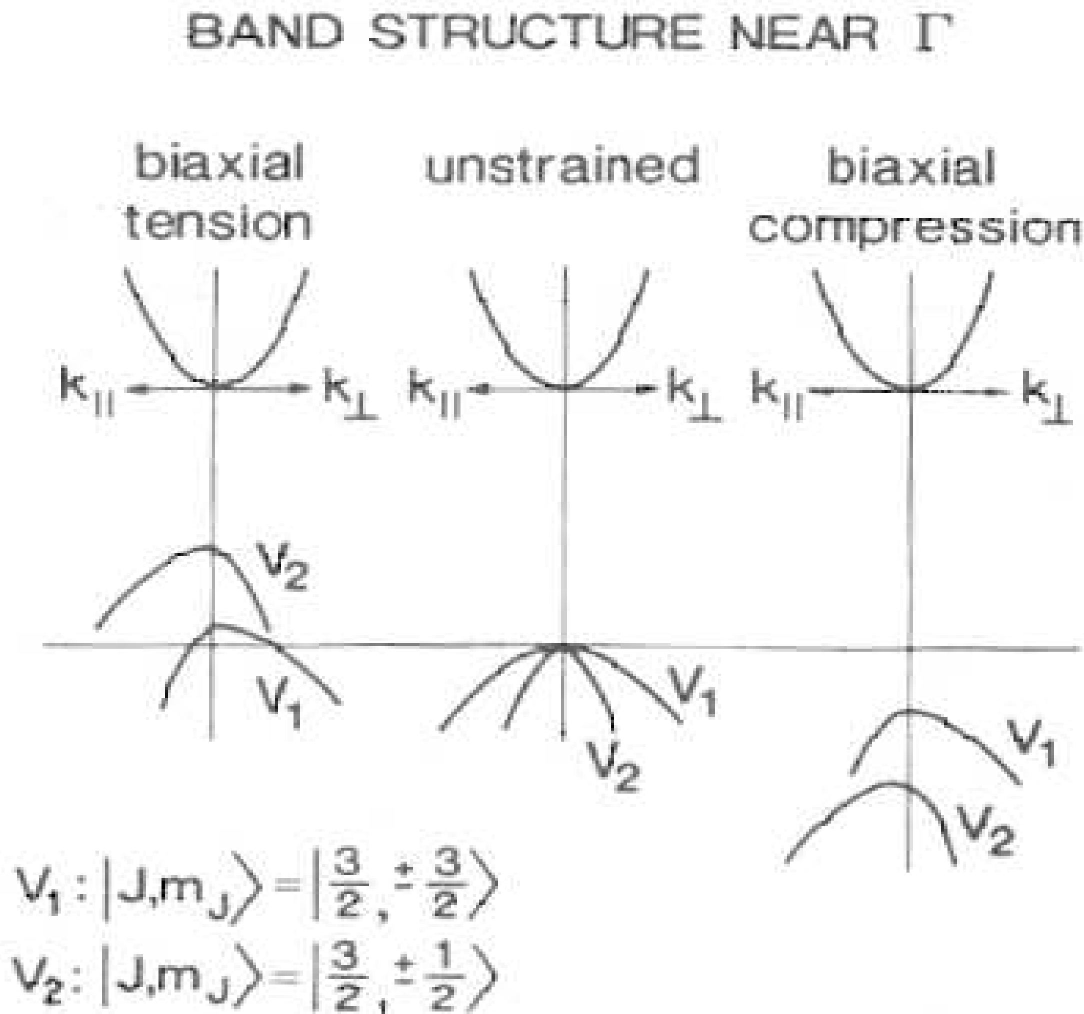

Figure 5.3: Schematic showing the effect of strain on semiconductor energy bands

These preliminary investigations of highly strained $In_xGa_{1-x}As/GaAs$ QW systems has already shown the complex nature of strain induced intermixing and has opened the way for many more indepth studies on the effects strain has on intermixing and possible applications to optoelectronic devices.

Chapter 6

Conclusion

The aim of studying Boron implantation in to the GaAs/$Al_xGa_{1-x}As$ QW system was to investigate the intermixing mechanisms present in a medium mass ion implanted QW system and compare these results with those gained for high and low mass ion implantation. The GaAs/$Al_xGa_{1-x}As$ system was chosen due to its lack of inbuilt lattice strain, so when the correct implantation dose and energies were used, the effects of various ion masses on intermixing extent could be compared.

The results obtained from the high and low mass ion implantation experiments reconfirmed a number of results for both dose and temperature dependent implantation. Both H and As ions were shown to produce good energy shift increases with increasing dose, and explanations for the two intermixing mechanisms dominant in each case were presented. The observation of a saturation in the energy shift for the high mass ion, but no corresponding saturation in the low mass ion case was indicitive of fundamentally different intermixing mechanisms for the different mass ions. Temperature dependent studies of H and As also reconfirmed previous results. Low mass ion implantation energy shift declined with temperature rise, due to the susceptability of point defects to dynamic annealing effects with elevated implantation temperature. The high mass ions showed a very small increase in energy shift with increase in temperature, indicating that the point defect clusters in the material were thermally stable in the temperature range investigated.

Boron implantation exhibited low energy shifts for the range of doses studied, and two hypotheses were put forward to explain the observed shifts. Further experimental work was carried out to test one possible mechanism (the binding of B with point defects in the material), however the results from this were found to be inconclusive, and further study is required on other medium mass ions to compare their intermixing induced shifts with those of Boron in order to better understand the mechanisms involved in medium mass implantation induced intermixing,

For a set implantation dose, Boron showed no appreciable temperature dependence, a feature that could serve to be useful during implantation as thermal changes would not cause error in the extent of intermixing created.

Study of the highly strained $In_xGa_{1-x}As$/GaAs QW system with 30% and 50% In content of the group III elements in the barrier layers aimed to investigate the role of strain in intermixed systems. It was found that strain relaxation induced red shifting was a prominant feature in the resulting PLS shifts, and that it directly competed with the blue shifting caused by defect diffusion between well and barrier layers.

Further study is warranted on the intermixing mechanisms present in GaAs/$Al_xGa_{1-x}As$

Boron implanted QW systems, for complete understanding of the mechanisms that resulted in supression of the intermixing. As well as this, further study on other medium mass ions is needed to help fully understand the intermixing mechanisms present between high and low mass ions.

The strain effects in the $In_xGa_{1-x}As/GaAs$ QW system produced some interesting preliminary results, and further work in this area would look to identify trends in dose and temperature dependence, and would look at ways in which the inbuilt strain may be utilised in optoelectronic applications.

Bibliography

[1] L.Esaki and R. Tsu, "Superlattice and negative conductivity in semiconductors," *IBM J. Res. Develop.*, pp 61-65 Jan. 1970

[2] Stephen Grey, "Philosophical Transactions of the Royal Society", **37**, 1731-32

[3] Dr Michael Shur, http://nina.ecse.rpi.edu/shur/SDMI/Notes/Noteshtm /02introduction/sld002, August 1998.

[4] Dr Michael Shur, http://nina.ecse.rpi.edu/shur/SDMI/Notes/Noteshtm /02introduction/sld003, August 1998.

[5] Felix Bloch, *Z. Physik*, **52**, 555 (1928).

[6] John Orton, "Superlattice Surprises" *Physics World* **2**, pp 39-42, July 1989.

[7] W. Laidig, N. Holonyak Jr., M. Camras, K. Hess, J. Coleman, P. Dapkus and J. Bardeen, "Disordering of an AlAs-GaAs superlattice by impurity diffusion," *Appl. Phys. Lett***38**, 776-778 (1981).

[8] Nick Holonyak Jr., "Impurity-induced layer disordering of quantum well heterostructures, discovery and prospects," *IEEE Selected topics in Quantum Electronics* **4**, 4 584 (1998).

[9] T. Schlesinger and T. Keuch, "Determination of the interdiffusion of Al and Ga in undoped (Al,Ga)As/GaAs quantum wells," *Appl. Phys. Lett.* **49**, 519-521 (1986).

[10] E. Koteles, B. Elman, P. Melman, J. Chi and C. Armiento, "Quantum well shape modification using vacancy generation and rapid thermal annealing" *Opt. Quantum Elecronics* **23**, S779-S787 (1991)

[11] B. Ooi, K. McIlvaney, M. Street, A. Helmy, S. Alying, A. Bryce, J. Marsh and J. Roberts, "Selective quantum well intermixing in GaAs/AlGaAs structures using impurity free vacancy diffusion" *Journal of Quantum Electronics* **13**, 1784-1793 (1997)

[12] A. McKee, C. McLan, A. Bryce, R. De La Rue, J. Marsh and C. Button, "High quality wavelength tuned multi-quantum well InGaAs/InGaAsP lasers fabricated using photoabsorption induced disordering," *Appl. Phys. Lett.***65**, 2263 (1994)

[13] C. McLean, A. McKee, G. Lullo, A. Bryce and R. De La Rue, "Quantum well intermixing with high spatial selectivity using a pulsed laser technique," *Electronic Lett.* **31**, 1285 (1995)

[14] Fu Lan "Quantum well intermixing in (In)GaAs/(Al)GaAs materials and devices," PhD Thesis, Dept. of Electronic Materials Engineering, ANU (2001)

[15] H. H Tan "Ion Beam Effects in GaAs/AlGaAs Materials and Devices," PhD Thesis, Dept. of Electronic Materials Engineering, ANU (1996)

[16] David K. Ferry and Robert O. Grondin, "Physics of Submicron Devices," pp 272, *Plenum Press, NY* (1991)

[17] David K. Ferry and Robert O. Grondin, "Physics of Submicron Devices," pp 273, *Plenum Press, NY* (1991)

[18] Bart J. Van Zegnbroeck, http://ece-www.colorado.edu/ bart/book/eband3.htm (1997)

[19] A. H. Wilson "The Theory of Metals," Cambridge, London (1954)

[20] Ming-Fu Li "Modern Semiconductor Quantum Physics," *World Scientific Publishing Co. Pte. Ltd*, pp 4-58, (1994)

[21] Ming-Fu Li "Modern Semiconductor Quantum Physics," *World Scientific Publishing Co. Pte. Ltd*, pp 175, (1994)

[22] Ming-Fu Li "Modern Semiconductor Quantum Physics," *World Scientific Publishing Co. Pte. Ltd*, pp 190, (1994)

[23] Ming-Fu Li "Modern Semiconductor Quantum Physics," *World Scientific Publishing Co. Pte. Ltd*, pp 191, (1994)

[24] J.S. Williams and J.M. Poate, "Ion induced damage and dynamic annealing processes," *Trans. Mater. Res. Soc. Jpn.*, **17,** pp 417-423 (1994)

[25] G.F Redinbo, H.G Craighead and J.M Hong, "Proton inplantation intermixing of GaAs/AlGaAs quantum wells," *J. Appl. Phys.*, **74**, pp 3099-3102 (1993)

[26] S. Eshlaghi, C. Meier, D. Suter, D. Reuter and A.D. Wieck, "Depth Profile of the Implantation Enhanced Intermixing of Ga Focused Ion Beam in AlAs/GaAs Quantum Wells," *J. Appl. Phys.* **86,** 11 (1999)

[27] J.W. Matthews and A.E. Blakeslee, *J. Crystal Growth* **27,**118 (1974)